Disrupting N-glycan expression on tumor cells boosts chimeric antigen receptor T cell efficacy against solid malignancies

Beatrice Greco[1,2], Valeria Malacarne[3,4], Federica De Girardi[1], Giulia Maria Scotti[5], Francesco Manfredi[6], Elia Angelino[3,4], Camilla Sirini[1,2], Barbara Camisa[1,6], Laura Falcone[1], Marta Angiola Moresco[1], Katia Paolella[1†], Mattia Di Bono[1,6], Rossana Norata[7], Francesca Sanvito[8], Silvia Arcangeli[1], Claudio Doglioni[2,8], Fabio Ciceri[2,9], Chiara Bonini[2,6], Andrea Graziani[3,4], Attilio Bondanza[1,2†], Monica Casucci[1*]

[1]Innovative Immunotherapies Unit, Division of Immunology, Transplantation and Infectious Diseases, IRCCS San Raffaele Scientific Institute, 20132 Milan, Italy.

[2]Vita-Salute San Raffaele University, 20132 Milan, Italy.

[3]Lipid Signaling in Cancer and Metabolism Unit, Division of Experimental Oncology, IRCCS San Raffaele Scientific Institute, 20132 Milan, Italy.

[4]Department of Molecular Biotechnology and Health Sciences, Molecular Biotechnology Center, University of Turin, 10124 Torino, Italy.

[5]Center for Omics Sciences, IRCCS San Raffaele Scientific Institute, 20132 Milan, Italy.

[6]Experimental Hematology Unit, Division of Immunology, Transplantation and Infectious Diseases, IRCCS San Raffaele Scientific Institute, 20132 Milan, Italy.

[7]San Raffaele Telethon Institute for Gene Therapy, IRCCS San Raffaele Scientific Institute, 20132 Milan, Italy.

[8]Pathology Unit, Division of Experimental Oncology, IRCCS San Raffaele Scientific Institute, 20132 Milan, Italy.

[9]Hematology and Hematopoietic Stem Cell Transplantation Unit, IRCCS San Raffaele Scientific Institute, 20132 Milan, Italy.

[*]Corresponding author. Email: casucci.monica@hsr.it

† K. P.: Currently at AstraZeneca, Milan, Italy.

† A. B.: Currently at AstraZeneca plc, Cambridge, UK.

One Sentence Summary: Reducing the expression of N-glycans on tumor cells enhances the therapeutic potential of chimeric antigen receptor T cells against solid tumors.

Abstract

Immunotherapy with chimeric antigen receptor (CAR) engineered T cells showed exceptional successes in patients with refractory B cell malignancies. However, first-in-human studies in solid tumors revealed unique hurdles contributing to poor demonstration of efficacy. Understanding the determinants of tumor recognition by CAR T cells should translate into the design of strategies that can overcome resistance. Here, we show that multiple carcinomas express extracellular N-glycans, whose abundance negatively correlates with CAR T cell killing. By knocking out mannoside acetyl-glucosaminyltransferase 5 (*MGAT5*) in pancreatic adenocarcinoma (PAC), we showed that N-glycans protect tumors from CAR T cell killing by interfering with proper immunological synapse formation and reducing transcriptional activation, cytokine production, and cytotoxicity. To overcome this barrier, we exploited the high metabolic demand of tumors to safely inhibit N-glycans synthesis with the glucose/mannose analogue 2-Deoxy-D-glucose (2DG). Treatment with 2DG disrupts the N-glycan cover on tumor cells and results in enhanced CAR T cell activity in different xenograft mouse models of PAC. Moreover, 2DG treatment interferes with the PD-1–PD-L1 axis and results in a reduced exhaustion profile of tumor-infiltrating CAR T cells in vivo. The combined 2DG and CAR T cell therapy was successful against multiple carcinomas besides PAC, including those arising from the lung, ovary, and bladder, and with different clinically relevant CAR specificities, such as CD44v6 and CEA. Overall, our results indicate that tumor N-glycosylation regulates the quality and magnitude of CAR T cell responses, paving the way for the rational design of improved therapies against solid malignancies.

Introduction

Engineering T cells to express chimeric antigen receptors (CARs) targeting lineage-restricted antigens is an effective tool to treat B cell malignancies *(1–4)*. However, as the technology moves to solid tumors, clinical responses have not been as robust *(5)*. In this setting, the inefficient trafficking and infiltration to the tumor site, the presence of inhibitory signals, and the paucity of tumor-restricted antigens pose unique barriers to the therapeutic benefit of CAR T cells. Even when these features are successfully counteracted, the therapeutic potential of CARs depends on the ability to exert contact-dependent biological functions through the formation of a lytic immune synapse (IS) with tumor cells *(6)*. This multi-step process culminates with the accumulation of actin filaments, the convergence of lytic granules at the microtubule organizing center (MTOC), the polarization of granule-loaded MTOC and the final release of granules at the IS cleft *(7–9)*. As this process primarily relies on ligand-receptor interactions, antigen density and accessibility are both essential attributes defining the ultimate success of CAR T cell therapy *(10)*.

Glycosylation is one of the most frequently occurring protein modifications. Glycoproteins are generated through the covalent link of glycans to asparagine or serine/threonine residues. Here we focus on N-glycans, comprising a core of two N-acetylglucosamine (GlcNAc) and three mannose residues *(11)*. In normal cells, core structures undergo extensive processing by several glycosyltransferases, which poise the maturation of nascent glycoproteins toward high-mannose, hybrid or complex branched N-glycans *(12)*. Tumor cells display aberrant glycosylation, which manifests as a profoundly diverse extracellular glycan coat as compared to healthy cells. This coating, besides regulating fundamental biological events, may also negatively impact the magnitude of antitumor responses, either by masking neo-epitopes to immune cells or by interfering with immune cell functions *(13)* For instance, a tumor cell's sialic acid might shut down NK activation and favor polarization of macrophages to an immunosuppressive M2 phenotype through binding to Siglec receptors *(14, 15)*. In opposite scenarios, the tumor glycan coat provides specific markers that can be conveniently exploited for immunotherapeutic strategies, as depicted by the clinical application of

CAR T cells targeting the cancer-associated Tn-glycoform of Mucin 1 *(16)*. Increased β1-6 N-glycan branching is among the most frequent alterations occurring in cancer cells *(17)*. Such modification is due to the increased activity of N-acetylglucosaminyltransferase-V (GnT-V), which is encoded by the mannoside acetyl-glucosaminyltransferase 5 (*MGAT5*) gene *(18)*. Expression of *MGAT5* is positively regulated by the Ras-Raf-Ets signaling pathway, which is commonly altered in tumors, and contributes directly to cancer growth, invasion, and metastasis *(19, 20)*. For example, *MGAT5* deficiency in glycosylation mutants of metastatic tumor cell lines impairs invasive potential *(20)*. In contrast, its overexpression correlates strongly with acquisition of metastatic features in a non-metastatic model of murine mammary carcinoma *(21)*. Interestingly, MGAT5 glycan products have been described in breast and colorectal carcinomas, where they correlate with decreased survival and poor prognosis *(22, 23)*.

We previously developed a CAR specific for the variant isoform 6 of CD44 (CD44v6*) (24, 25)* for the treatment of acute myeloid leukemia (AML) and multiple myeloma (MM). More recently, CD44v6 CAR T cells have also proved efficacy in xenograft models of lung and ovarian carcinoma, paving the way for a wider exploitation toward solid tumors *(26)*. CD44v6 is a heavily glycosylated protein, a feature shared with several solid tumor CAR antigens, including the Carcinoembrionic antigen (CEA), which is currently under investigation in patients with primary or metastatic pancreatic carcinoma *(27–29)*. Most commonly, CAR T cells engage their antigen through a monoclonal antibody (mAb)-derived binding moiety. Glycosylated proteins encompass different types of antigenic epitopes. Glycopeptidic epitopes are defined by antibodies recognizing oligosaccharide units and adjacent amino acid residues as opposed to peptidic epitopes, which are recognized both in fully and partially glycosylated antigens *(30)*. For example, the BIWA-8 mAb, which was used to construct the 44v6.28ζ CAR's single chain fragment variable (scFv), falls in the latter category, as it recognizes a peptidic epitope lacking the canonical consensus sequence for N-glycosylation *(31)*. Nevertheless, especially in richly glycosylated proteins, glycosylation of one or more flanking amino acids can mask mAb binding, as has been reported for the influenza virus

hemagglutinin, the human Mucin 1 (MUC1) protein and, more recently, Programmed death-ligand 1 (PD-L1) *(32–34)*. Because glycosylation is one of the most frequently occurring protein modifications, this characteristic might become highly relevant while dissecting the factors regulating CAR T cell activity. Interestingly, preclinical evaluations of CAR T cell efficacy toward solid tumors have generally not taken this feature into account.

In this study, we generated N-glycosylation defective pancreatic tumor cells by knocking-out the expression of the glycosyltransferase *MGAT5* and exploited CD44v6 and CEA CARs to model the impact of tumor N-glycans on the targeting of tumor cells by CAR T cells. To safely address this barrier, we tested the combination of CAR T cell treatment with the glucose/mannose analogue 2-deoxy-D-glucose (2DG), known for its ability to preferentially accumulate in tumors over healthy cells *(35, 36)*. The results obtained unravel facets of the biology of tumor recognition by CAR T cells and instruct the development of improved strategies for the treatment of solid malignancies.

Results

Branched N-glycans shield pancreatic tumors from 44v6.28ζ targeting.

Pancreatic adenocarcinoma (PAC) has an extremely poor prognosis and limited therapeutic options. Contrary to expectations, CAR T cell therapy has also failed to achieve responses *(29)*, requiring the development of more sophisticated strategies. In order to decipher the biological impact of N-glycans in PAC tumors, we analyzed the mutational burden of the glycosyltransferases involved in the synthesis of these sugar moieties. We found that 19% of patients from cBioportal *(37, 38)* carried genomic alterations in glycosyltransferases involved in the synthesis of N-glycans (fig. S1A), and this feature associated with poor outcomes (fig. S1B). Comparative analysis further identified a similar mutational burden among genes specifically accounting for either branched or high-mannose N-glycan subtypes (Fig. 1A and fig. S1C). However, genes involved in branched N-glycan synthesis alone associated with markedly worsened disease-free survival, thus providing evidence that alterations of these sugar structures endow PAC cells with increased aggressiveness (Fig. 1B and fig.

S1D). Interestingly, most of these alterations were amplifications (Fig. 1C), supporting the greater abundance of branched N-glycans in malignant cells *(20)*. To measure the expression of N-glycosyltransferases accounting for branched N-glycans elongation, we analyzed RNA sequencing data of PAC specimens from the Cancer Genome Atlas (TCGA). GSEA analysis *(39)* showed a marked enrichment of this pathway in patients as compared to healthy controls (Fig. 1D).

Among enriched genes, *MGAT5* encodes for a Golgi enzyme pivotal for branched N-glycans biosynthesis and responsible for the increased β1-6GlcNAc-branching that notoriously accompanies malignant transformation *(21)*. Therefore, to weigh the contribution of tumor branched N-glycans to the targeting by CAR T cells, we knocked-out the expression of *MGAT5* in T3M-4 PAC cells, thereby preventing β1-6 elongation whilst preserving core sugars (Fig. 1E). This pattern was confirmed by decreased binding to Phytohemagglutinin-L lectin (PHA-L), which specifically marks MGAT5 glycan products, concurrent with increased Concanavalin A staining, that reveals mannose residues (Fig. 1F and G). Reduced binding to PHA-L was further confirmed by immunohistochemistry, both at intracellular and surface level (Fig. 1H). By contrast, surface accessory molecule concentrations remained relatively stable, indicating no perturbations of the overall surface phenotype (fig. S2A). Similarly, no major differences emerged in the expression of CD44v6 (fig. S2B), which was selected as model CAR antigen being highly glycosylated and expressed on several solid tumors *(40)*.

To generate CAR T cells, T lymphocytes were stimulated with αCD3/CD28 beads, transduced with CD28-costimulated CARs specific for CD44v6 (44v6.28ζ) or control CD19 (19.28ζ) and expanded with interleukin (IL)-7 and IL-15, according to a protocol that preserves T cell fitness *(41–43)*. The effect of *MGAT5* knock-out on tumor recognition by 44v6.28ζ cells was analyzed in co-culture experiments at different effector-to-target (E:T) ratios. Hampering branched N-glycans in T3M-4 PAC cells dramatically enhanced antitumor efficacy by CAR T cells, marked by increased cytolytic activity (Fig. 1I), secretion of interferon (IFN)-γ and tumor necrosis factor (TNF)-α (Fig. 1J). These findings were corroborated with the N-glycosylation inhibitor tunicamycin that abrogates core N-

glycans synthesis, further underscoring the negative impact of these sugar structures on tumor cell targeting by CAR T cells (fig. S2C and D).

Impairing the synthesis of MGAT5 N-glycan products in pancreatic tumors improves functional engagement by CAR T cells.

To investigate the basis for the enhanced antitumor efficacy toward N-glycosylation-defective cells, we examined limiting steps of the targeting process by CAR T cells, reasoning that N-glycans removal would alter the quality and strength of tumor recognition. As previously reported, the quality of the immunological synapse (IS) predicts antitumor activity of CAR T cells *(6)*. Accordingly, we characterized the IS formed between CAR T cells and either wild-type or *MGAT5* knocked-out T3M-4 tumor cells. The IS was reconstituted and visualized as maximum projection of 0.2 um z-stack and quantification analysis was performed as previously described *(44)*. Remarkably, T3M-4 cells devoid of MGAT5 glycan products engaged in a superior IS with 44v6.28ζ cells, featuring higher F-actin accumulation, stronger granule convergence, and reduced distance of microtubule-organizing-center (MTOC) to F-actin (Fig. 2A and B), three well established parameters for functional cytolysis *(9, 45)*. No such differences were observed in control 19.28ζ cells (fig. S3A).

Because IS strength dictates the degree of T cell activation *(6)*, we examined whether N-glycosylation-defective tumors would elicit a stronger functional engagement by CAR T cells. To this aim, we analyzed intracellular signaling events by exploiting a triple-parameter-reporter (TPR) Jurkat cellular model, which allows measuring transcriptional activity through the expression of fluorescent proteins *(46)*. TPR Jurkat cells were transduced to express either 44v6.28ζ or 19.28ζ constructs and stimulated with wild-type or *MGAT5* knocked-out T3M-4 tumor cells (Fig. 2C). Importantly, N-glycosylation-defective tumors induced stronger calcineurin-nuclear factor of activated T cells (NFAT) and nuclear factor kappa B (NF-κB) signals in 44v6.28ζ^+ TPR Jurkat cells (Fig. 2D). In contrast, Activator protein 1 (AP-1) appeared to be poorly informative, so we relied on

NFAT and NF-κB for further investigations (fig. S3B). The specificity of this effect was confirmed by the lack of signal in 19.28ζ^{+} TPR Jurkat cells (fig. S3C). Overall, these findings support a mechanism of tumor resistance to CAR T cell therapy that place tumor engagement and CAR signaling strength under the control of malignant branched N-glycans.

Prophylactic treatment with 2DG sensitizes pancreatic tumors to 44v6.28ζ targeting.

To pharmacologically overcome the glycosylation barrier, we employed the glucose/mannose analogue 2-Deoxy-D-glucose (2DG). Although 2DG is mainly known for its capacity to block glycolysis through hexokinase and phosphoglucose isomerase inhibition *(47)*, its interference with N-linked glycosylation has also been reported. 2DG competes with mannose and incorporates into lipid-linked oligosaccharides (LLOs) of nascent glycoproteins, overall causing an aberrant glycosylation status *(48)*.

Treatment with 2DG inhibited branched N-glycans expression in T3M-4 cells, as indicated by reduced PHA-L binding (Fig. 3A). Interestingly, this effect manifested at concentrations of 2DG as low as 2mM and 4mM, which were less effective in driving glycolytic flux as measured by cellular lactate production (fig. S4A). Hence, based on our results and previously reported findings *(48)*, we relied on 4mM 2DG for subsequent evaluations and functional testing. Inhibition of glycosylation usually triggers endoplasmic reticulum (ER) stress due to the accumulation of unfolded and degraded proteins. Accordingly, treatment of T3M-4 tumors with either tunicamycin or 2DG showed a clear upregulation of the ER stress marker GRP78 by western blot analysis. This effect was reverted by addition of mannose, but not glucose, and was not induced by 2FDG, which preferentially blocks glycolysis, confirming that 2DG inhibits N-glycosylation by mannose mimicry. Interestingly, the same result was not observed for *MGAT5* knocked-out cells, possibly suggesting that 2DG causes a more potent glycosylation interference compared to the *MGAT5* deficiency (Fig. 3B).

To gain further insights into the dynamic activity of 2DG in T3M-4 cells, we analyzed the kinetics of de-glycosylation and re-glycosylation upon treatment. PHA-L binding was abrogated within 18

212 hours of initial exposure to 2DG (fig. S4B). Binding was restored by 18 hours after treatment wash-
213 out, showing rapid de-glycosylation and re-glycosylation kinetics (fig. S4B). Before proceeding with
214 functional testing, we assessed the effects of 2DG-mediated de-glycosylation on the surface exposure
215 of tumor antigens, which is a crucial requirement for CAR T cell targeting. Although CD44v6 and
216 β1 integrin stained positive (fig. S4C), biotinylation assay of surface proteins showed a molecular
217 weight shift compatible with extensive de-glycosylation (Fig. 3C). Accordingly, N-glycans removal
218 through treatment with PNGase F produced comparable results, suggesting that 2DG treatment allows
219 surface exposure of proteins deprived of sugar structures.
220 We then explored the ability of 2DG to sensitize tumors to CAR T cell targeting. Notably, 2DG-
221 treated T3M-4 cells were more efficiently killed by 44v6.28ζ cells (Fig. 3D) and elicited a stronger
222 transcriptional engagement in 44v6.28ζ but not 19.28ζ TPR Jurkat cells (Fig. 3E and fig. S4D).
223 Treatment with low dose 2DG alone did not interfere considerably with tumor cell proliferation or
224 survival (fig. S4E and F). To support that this effect is truly accountable to inhibition of mannose (N-
225 glycosylation) rather than glucose (glycolysis) pathway by 2DG, we performed co-culture
226 experiments supplementing each sugar individually. Whereas addition of glucose did not alter the
227 improved tumor cell killing following treatment with 2DG and 44v6.28ζ cells, exogenous mannose
228 blocked the effect of 2DG exposure (Fig. 3F). Importantly, treatment of T3M-4 cells with 2FDG did
229 not increase killing by CAR T cells, ultimately pointing at inhibition of tumor glycosylation as the
230 main underlying mechanism of action (Fig. 3F).
231 This treatment combination was then investigated in a xenograft mouse model of PAC, whereby
232 engrafted T3M-4 retained high expression of branched N-glycans (fig. S4G). In this model, T3M-4
233 cells were transduced to express a secreted luciferase, which allows the easy monitoring of tumor
234 progression by serial peripheral blood analysis *(49)*. To test the potency of the combined approach,
235 we exploited both a permissive and a more challenging in vivo setting, the former with low tumor
236 burdens and high CAR T cell doses, the latter with high tumor burdens and low CAR T cell doses

(Fig. 3G). In both settings, 2DG was administered prior CAR T cell infusion to sensitize tumors to CAR T cell assault. In the context of low tumor burden, tumor control was achieved regardless of 2DG treatment (Fig. 3H). In the high tumor burden model, however, tumor growth was controlled more effectively in mice treated with 44v6.28ζ cells and 2DG (Fig. 3H). Notably, improved efficacy was associated with a reduced exhaustion profile of tumor-infiltrating 44v6.28ζ cells. We observed a significantly lower frequency of cells expressing one or more inhibitory receptors such as T-cell immunoglobulin domain and mucin domain 3 (TIM-3), lymphocyte activating 3 (LAG-3), programmed cell death protein 1 (PD-1) and CD57 (SPICE analysis P=0.001, Fig. 3I and fig. S4H). N-glycosylation was reported to be crucial for co-inhibitory ligand-receptor pair bindings, including programmed death-ligand 1 (PD-L1)-PD-1, poliovirus receptor (PVR)-T-cell immunoreceptor with Ig and ITIM domains (TIGIT), galectin-9 (Gal9)-TIM-3, cytotoxic T-Lymphocyte associated protein 4 (CTLA4)-the cluster of differentiation 80 (CD80 or B7-1) and CTLA4- cluster of differentiation 86 (CD86 or B7-2). Among these, the PD-L1-PD-1 interaction underwent the most substantial loss upon N-glycans removal *(50, 51)*. Considering the relevance of blocking this inhibitory axis from a clinical standpoint, we tested whether 2DG-induced tumor de-glycosylation would directly impede the PD-1–PD-L1 interaction. Interestingly, western blot biotinylation assay of surface proteins from PD-L1$^+$ T3M-4 cells revealed a marked shift in PD-L1 weight upon treatment with 2DG, which is compatible with de-glycosylation (Fig. 3J). Accordingly, upon treatment with 2DG, PD-L1$^+$ T3M-4 cells exhibited a significant decrease in the ability of binding to recombinant human PD-1 (P=0.024, Fig. 3K). These findings suggest that combination with 2DG not only improves tumor clearance but might also enable CAR T cells to evade immune checkpoint inhibition.

Due to metabolic deregulation, 2DG should preferentially accumulate in tumors rather than healthy tissues *(47, 52)*. To substantiate this assumption, we examined the effects of 2DG on healthy keratinocytes as putative site of on-target off-tumor reactions by 44v6.28ζ cells. A biotinylation assay of surface proteins confirmed an invariant glycosylation status of primary keratinocytes upon

treatment with 2DG (fig. S5A). Accordingly, cytotoxicity of 44v6.28ζ cells also remained negligible toward 2DG-treated primary keratinocytes (fig. S5B). A similar pattern was observed in peripheral blood mononuclear cells, where exposure to 2DG had no effect on either PHA-L binding and the overall survival (fig. S5C and D).

Co-treatment with 2DG prolongs the survival of pancreatic tumor-bearing mice receiving 44v6.28ζ cells.

To explore combinatorial regimens, we previously administered 2DG prior to CAR T cell transfer in order to sensitize solid tumors to killing by CAR T cells (Fig. 3D to I). However, the short-term effect on N-glycosylation observed after 2DG treatment could impair long-term benefit of CAR T cell treatment. We therefore proceeded to test a combinatorial regimen comprising prolonged treatment with 2DG. This differs from the previous setting in which 2DG was administered beforehand to tumor alone. Therefore, it became crucial to test the potential accumulation of 2DG in CAR T cells and identify if there were any consequent effects. To this aim, we used the fluorescent glucose analogue (2-(N-(7-nitrobenz-2-oxa-1,3-diazol-4-yl)amino)-2-deoxyglucose (2-NBDG) as a tracer to quantify glucose uptake in living cells *(53, 54)*. 2NBDG uptake was evident in resting T cells and, expectedly, more so in 44v6.28ζ cells activated through polyclonal stimulation with αCD3/CD28 (Fig. 4A). However, when 44v6.28ζ cells were challenged with target BxPC-3 tumor cells in co-culture, 2NBDG uptake was highly skewed toward the tumor (Fig. 4B). This phenomenon occurred despite marked T cell activation, as confirmed by CD69 upregulation in 44v6.28ζ cells compared to control T cells (Fig. 4C). Accordingly, whereas lactate production was reduced upon treatment of polyclonally activated 44v6.28ζ cells with 2DG in vitro (fig. S6A), no such alteration was observed in 44v6.28ζ cells retrieved from tumor masses of mice receiving 2DG (fig. S6B). Overall, these data point to a preferential accumulation of 2DG in tumors during co-treatment regimens and suggest that there are only minor direct effects on CAR T cells. Importantly, we also

observed that cytotoxicity was associated with glycosylation blockade by 2DG in this treatment setting, as addition of exogenous mannose, but not glucose, reverted the effect of 2DG treatment and 2FDG failed to synergize with 44v6.28ζ cells (Fig. 4D).

We then tested the prolonged co-treatment of 2DG and 44v6.28ζ cells in high tumor burden PAC xenograft models (Fig. 4E). In T3M-4 xenografts, treating mice with repetitive injections of 2DG alone proved ineffective, as opposed to 44v6.28ζ cells that achieved a significant survival benefit (T3M-4 versus T3M-4+2DG P=0.4945; T3M-4 versus 44v6.28ζ P=0.0010). However, the combination of 2DG and 44v6.28ζ cells afforded the most durable tumor control, outperforming both individual treatments (T3M-4+2DG versus 44v6.28ζ+2DG P=0.0003, Fig. 4F). This result was confirmed in BxPC3 xenografts, in which the combined therapy provided the best therapeutic potency, significantly prolonging the survival of mice compared to either single treatment alone (BxPC3 versus BxPC3+2DG P>0.9999; BxPC34 versus 44v6.28ζ P=0.3523; BxPC3+2DG versus 44v6.28ζ+2DG P=0.0047, Fig. 4G). In both models, $CD8^+$ CAR T cells expanded robustly at early time points and contracted over time in favor of $CD4^+$ T cells, regardless of the 2DG combination (fig. S7A and B). Prominent phenotypical differences emerged in the late phase of the immune response in mice receiving the combined therapy. The persisting progeny of circulating 44v6.28ζ cells from 2DG-treated mice comprised a higher percentage of early-differentiated $CD62L^+CD45RA^+$ stem cell memory T (T_{SCM}) cells or $CD62L^+CD45RA^-$ central memory T (T_{CM}) cells, at the expense of $CD62L^-CD45RA^-$ effector memory T (T_{EM}) cells or $CD62L^-CD45RA^+$ terminal effector (T_{EMRA}) T cells (Fig. 4H). To expand the characterization of tumor-infiltrating (TIL) CAR T cell fitness in the co-treatment regimen, we interrogated the co-expression of multiple exhaustion and activation markers with Barnes-Hut Stochastic Neighbor Embedding (BH-SNE) *(55)* and Kmeans clustering through a data optimization and deconvolution workflow *(56, 57)*. The analysis identified distinctive phenotypic clusters of 44v6.28ζ TILs deriving from the two treatment conditions (fig. S8A and B, Fig. 4I). Cluster analysis revealed that 44v6.28ζ TILs retrieved from mice

receiving 2DG exhibited a reduced exhaustion profile, characterized by a lower expression of multiple inhibitory receptors, either considered alone as shown by heat map visualization (Fig. 4J) or in combination (Fig. 4K). These data further support the multifaceted benefit of combining 2DG and CAR T cells.

Co-treatment with 2DG improves CAR T cell efficacy against multiple carcinomas.

To examine the exploitability of the combined therapy, we screened N-glycans expression in a panel of cell lines deriving from different human carcinomas. PHA-L binding analysis revealed that besides PAC, tumors arising from lung and bladder also express N-glycans (Fig. 5A). Of note, the combination with 2DG markedly increased killing of highly glycosylated tumors that are hardly targeted by 44v6.28ζ cells alone, such as 5637 cells, while having marginal effects on poorly glycosylated tumors efficiently recognized by CAR T cells, such as MDA-231 cells (Fig. 5A and fig. S9A). Correlative analysis of CD44v6^{+} tumors challenged with CAR T cells revealed that antigen expression failed to fully predict the degree of target cell killing; on the contrary, N-glycan expression assessed through PHA-L binding showed a strong negative association (Fig. 5B) and predicted the effectiveness of the combined therapy (fig. S9B), supporting the central role of this post-translational modification in defining susceptibility to CAR T cell targeting.

To expand the assessment of the therapeutic potential with multiple tumors, we employed a model of bladder carcinoma (5637 cells) and of ovarian (IGROV-1 cells) carcinoma. Importantly, in line with previous observations from T3M-4 PAC tumors, treatment with 2DG induced extensive PD-L1 de-glycosylation (Fig. 5C) and robustly decreased binding of PD-1 to tumor-expressed PD-L1 (Fig. 5D). In both tumor xenograft models, 2DG proved ineffective whereas 44v6.28ζ cells, either as monotherapy or in combination with 2DG, were equally capable of eliciting potent antitumor responses, leading to marked tumor clearance. However, the superiority of the combined treatment was confirmed by the unique capacity to elicit effective recall responses after tumor rechallenge, suggesting long-term protection from relapse (Fig. 5E and F). Consistent with previous findings,

persistent 44v6.28ζ cells isolated from mice receiving 2DG injections featured increased proportions of early memory T cells (fig. S10A and B). In contrast, 44v6.28ζ alone readily acquired an effector memory phenotype, possibly accounting for the inadequate control of tumor rechallenge.

To confirm the broad exploitability of the combined treatment toward different tumors, we analyzed genomic mutational burden and RNA sequencing data of hallmark enzymes for N-glycan synthesis in patients with different types of carcinomas using cBioportal and TCGA data. As anticipated from cell line screening, N-glycosyltransferases were found mutated (fig. S11) and upregulated (Fig. 5G) in many tumor specimens compared to corresponding normal tissue samples, including several tumors already targeted by CAR T cells in clinical trials. Although each specific tumor indication will certainly require dedicated pharmacokinetic and pharmacodynamic studies, these results support the inclusion of 2DG as a tool to improve the therapeutic outcome of 44v6.28ζ cells toward multiple carcinomas.

2DG boosts the antitumor efficacy of CEA.28ζ cells.

We next examined if removing N-glycans would be beneficial for CAR specificities other than CD44v6. To this aim, we generated T cells engineered to express a CD28-costimulated CAR targeting the Carcinoembrionic antigen (CEA.28ζ) *(27–29)*. Although glycosylated T3M-4 PAC cells were highly resistant to CEA.28ζ cells, knockout of *MGAT5* markedly enhanced tumor elimination and T cell activation (Fig. 6A and fig. S12A). Similar results were obtained when core sugar synthesis was inhibited with tunicamycin (fig. S12A and B). Accordingly, *MGAT5* knocked-out T3M-4 tumors induced stronger NFAT signals in CEA.28ζ^{+} TPR Jurkat cells compared to control N-glycosylation-competent cells (Fig. 6B). Treatment with 2DG confirmed and extended these results, showing increased targeting of T3M-4 tumor cells measured as killing (Fig. 6C), NFAT signaling (Fig. 6D), CD69 upregulation (fig. S12A) and IFN-γ production (fig. S12C). Importantly, the mechanism by which 2DG enhances CEA.28ζ functionality was confirmed to be related to interference of tumor

glycosylation rather than glycolysis, as addition of exogenous mannose prevented the benefit of 2DG treatment in both the prophylactic and co-treatment regimens (Fig. 6E and fig. S12D). Interestingly, the benefit from the 2DG combination was seemingly unrelated to the CAR design, as improved NFAT and NF-kB signaling was also evident when 4-1BB-costimulated CEA CARs (CEA.BBζ) were employed (fig. S12E). Importantly, the mechanism by which 2DG enhances CEA.28z functionality was confirmed to be related to interference of tumor glycosylation rather than glycolysis, as addition of exogenous mannose prevented the benefit of 2DG treatment in both the prophylactic and co-treatment regimens (Fig. 6E and fig. S12D). Similar to 44v6.28ζ cells, the uptake of 2NBDG was also skewed toward tumor cells, rather than activated CEA.28ζ cells, in co-culture experiments (Fig. 6F to H). Importantly, besides PAC cell lines, the combination of CEA.28ζ cells and 2DG proved effective against other cancer cell lines (Fig. 6I and fig. S12F), including lung and bladder cancer, further confirming the potential for a wide applicability of the proposed approach.

Discussion

In this study, we have demonstrated that N-glycans provide multifaceted protection to solid tumors from CAR T cell killing. Furthermore, we provide evidence that pharmacologic interventions inhibiting N-glycan synthesis, such as treatment with the glucose/mannose analogue 2DG, successfully offset this shield, restoring susceptibility to CAR T cell targeting toward several solid malignancies. The biology of tumor recognition by CAR T cells remains poorly unraveled. The relative resistance of solid tumors to CAR T cells has underscored the need for a thorough understanding of all possible determinants. Altered glycosylation is a hallmark of malignant transformation, frequently manifesting as incomplete synthesis of O-glycans and increased branching of N-glycans *(20, 21)*. Whereas the former provides neoantigens for CAR T cells *(16)*, cumbersome N-glycans may have a direct impact on tumor cell recognition. To shed light on this unexplored

388 subject, we fine-tuned the stepwise N-glycan elongation by knocking-out the glycosyltransferase
389 *MGAT5* from tumors. Using *MGAT5*-deficient tumor cells, we explored quantitative imaging of the
390 CAR lytic synapse and analysis of transcription factor activation. We demonstrated that extracellular
391 branched N-glycans allow cancer cells to resist CAR T cell killing by increasing their activation
392 threshold and interfering with immunological synapse formation ab initio. Importantly, the N-glycan
393 shield applies to several types of carcinomas and CAR antigen specificities, not only revealing that
394 evaluation of target expression is insufficient to infer the potency of killing but also identifying N-
395 glycans as an actionable target for pharmacological intervention. Accordingly, we observed a clear
396 negative correlation between N-glycan expression and the potency of killing by CAR T cells,
397 warranting the potential adoption of N-glycan expression as a predictive biomarker for the screening
398 of patients who are likely to resist CAR T cell treatment and might benefit from de-glycosylating
399 strategies.
400 Consistent with previous studies, the glycan shield might act in multiple ways, either by direct
401 masking of antigenic epitopes or by hindering close cell-to-cell proximity. This last feature is a pillar
402 of the kinetic segregation model for T cell receptor (TCR) triggering, which postulates that close cell-
403 to-cell apposition sustains enhanced T cell activation by causing the passive marginalization of
404 phosphatases, such as CD45, which no longer counteracts kinase activities *(58)*. Recently, this model
405 has proved valid also for bispecific antibodies *(59)*, supporting the assumption that tumors with bulky
406 extracellular glycans might be suboptimal for lytic immune synapse formation with CAR T cells.
407 From our studies, short-term in vitro mechanistic evaluations strongly point at direct antigen
408 engagement and cell-to-cell proximity as two major forces driving differential tumor cell killing in
409 the presence or absence of N-glycans. However, the specific contribution of either of the two will be
410 the object of future studies. Conversely, accessory molecules shape the quality and duration of
411 antitumor responses in the long-term. In particular, signaling by immune checkpoint molecules is a
412 well-documented mechanism of resistance to T cell killing posed by solid tumors. In line with this
413 notion, CAR T cell therapy can greatly benefit from disruption of inhibitory pathways, either through

checkpoint blockades or by pursuing genetic strategies for counteracting their signaling *(60, 61)*. Interestingly, it has been recently reported that N-glycosylation ensures proper functionality of co-inhibitory ligand–receptor pairs, including the PD-L1–PD-1 axis, while being dispensable for co-stimulatory signaling, hence directly driving cancer-cell mediated immunosuppression *(50)*. Accordingly, we show here that treatment with 2DG abrogates binding of PD-1 to PD-L1-expressing tumors. Moreover, in two mouse models of PAC, we show that inhibition of tumor N-glycosylation skews effector cells to resist the damaging consequences of inhibitory signals, as indicated by decreased expression of exhaustion and senescence markers and robust cytotoxic effector response. Therefore, the beneficial effects of combining de-glycosylating agents to CAR T cells might be at least two-fold, either to be ascribed to a superior immunological synapse or to the disruption of checkpoint signaling pathways.

In this study, we demonstrated that tumor treatment with tunicamycin resembles the phenotype of MGAT5 knocked-out cells, supporting the key role of N-glycans in the resistance of tumors to CAR T cell activity. However, in a translational effort toward a safe clinical applicability, we propose combinatorial treatment with 2DG to overcome the glycosylation barrier. Differently from other de-glycosylating agents entering cells indiscriminately, 2DG accumulates preferentially in tumors as a consequence from the Warburg effect *(35)*. This characteristic is exploited in cancer diagnosis where radiolabeled 2DG (2-deoxy-2-[^{18}F]fluoro-D-glucose) is commonly used as a tracer in positron emission tomography (PET) scans. The selective responsiveness of tumors to 2DG is further supported by previous clinical experience proving good tolerability in solid cancers, either by itself or in combination with chemotherapy or radiotherapy, even during repetitive treatment schedules *(36, 62, 63)*. Most recently, the unique capacity of 2DG to accumulate in cells with high metabolic demand has led to its approval by the Indian government for emergency use as adjunct therapy to the standard of care in the treatment of patients with COVID-19 *(64)*. Accordingly, our results endorse the safety of this compound by showing that 2DG preferentially de-glycosylates tumors rather than healthy cells.

Although 2DG is commonly employed as glycolysis inhibitor, in our conditions (normoxia), its impact on tumor cells was seemingly unrelated to such effect, as no major cytostatic activity was observed *(65)*. To support that the synergy with CAR T cells was accountable to inhibition of mannose (N-glycosylation) rather than glucose (glycolysis) pathway by 2DG, we supplemented either sugar individually during killing assays. Whereas addition of glucose did not alter the synergy between 2DG and CAR T cells, exogenous mannose reverted such effect, pointing at inhibition of tumor glycosylation by mannose mimicry as the main underlying mechanism of action in our conditions. Nevertheless, within hypoxic tumor microenvironments, 2DG should likely induce cell death per se as a consequence from metabolic impairment, predicting that in some applications the effects of combining 2DG with CAR T cells might likely be superior to what reported from our results. At the same time, during co-treatment regimens, 2DG might have an impact on CAR T cells as well. The metabolic switch toward aerobic glycolysis also occurs in immune cells as well upon pro-inflammatory signals *(66)*. While it is known that glycolysis sustains highly proliferating effector T cells *(67)*, enforcing glycolytic metabolism was found to inhibit the generation of early memory $CD8^+$ T cells *(54)*. Accordingly, it has been reported that the ex vivo priming of $CD8^+$ T cells in the presence of glycolysis inhibitors, such as 2DG, favors the generation of long-lived memory $CD8^+$ cells displaying superior antitumor activity once transferred in vivo *(54)*. Although we observed a clear uptake of the fluorescent glucose analogue 2-NBDG in CAR T cells when cultured alone, which mirrored a marked decrease on lactate production upon treatment with 2DG in a dose-dependent fashion, no such effect was evident in T cells when the tumor was present, suggesting that 2DG has only marginal effects in CAR T cells. This phenomenon was observed when testing both 44v6.28ζ and CEA.28ζ cells in vitro and was further supported by the observation of an invariant intracellular lactate production in tumor infiltrating 44v6.28ζ cells retrieved from mice receiving 2DG co-treatment. Nonetheless, we observed a robust skewing toward an early memory phenotype in circulating CAR T cells from mice receiving prolonged 2DG. This finding is particularly appealing,

since clinical experience with CAR T cells identified early memory gene signature as one paramount determinant of therapeutic success *(68, 69)* and multiple strategies are currently underway to enrich and maintain CAR T cells with a stem and central memory phenotype *(43, 70)*. Although we have no proof of a direct accumulation of 2DG in peripheral CAR T cells during prolonged co-treatments, we might speculate that its inherent effect was anything but beneficial to the therapeutic outcome.

We recognize some potential limitations of our present study. First, we acknowledge the lack of functional results on patient-derived samples. However, the analysis of RNA sequencing data in patients with different types of carcinomas showed that N-glycans biosynthesis enzymes are upregulated in many tumor specimens, which suggest consistency with malignant cell lines functional results. Second, as anticipated above, the specific contribution of antigen versus de-glycosylation of other molecules remains unclear and will be the object of future studies.

In summary, we have demonstrated that extracellular N-glycans provide a potent tumor resistance mechanism by increasing the CAR T cell activation threshold and by promoting CAR T cell exhaustion. Our findings point to the therapeutic potential of combining CAR T cells with 2DG to counteract multiple layers of tumor resistance, including the inadequate tumor engagement and the damaging effects of inhibitory pathways (fig. S13). This knowledge has immediate translational opportunities and also provides new directions for the rational design of improved therapeutic approaches for solid tumors.

Materials and Methods

Study Design

The objective of this study was to analyze the impact of tumor N-glycosylation on the targeting by CAR T cells and to demonstrate that the combination with the glucose/mannose analogue 2DG safely potentiates the antitumor efficacy toward several carcinomas in vitro and in vivo. All in vitro experiments were performed with at least three different healthy donors and immunological synapse studies were performed by an operator who was blinded to group's allocation. In vivo experiments in NSG mice were performed with 3 to 9 mice per group based on previous experiments showing that this size could guarantee good reproducibility and emergence of statistically significant differences. No statistical methods were used to pre-determine sample size. Tumor-bearing mice were randomized into treatment groups before T cell infusion based on the amount of established tumors. Mice were treated by an operator who was blinded to treatment groups. All analysis in vitro and in vivo was based on objectively measurable data and the specific number of animals and experimental replicates are indicated in the figure legends.

Generation of CAR constructs

44v6.28ζ, 19.28ζ, CEA.28ζ and CEA.BBζ CARs contain specific single chain fragment variables (scFv) derived from BIWA-8, FMC63 and BW431-26 mAbs, respectively. All scFvs were synthetized by GeneArt (Thermo Fisher Scientific) as previously described *(25)* and cloned into an original CAR incorporating an IgG1-derived hinge spacer, a CD28 transmembrane and costimulatory domain and a CD3ζ endodomain *(71)*. To generate CEA.BBζ, the CD28 transmembrane and co-stimulatory domains were substituted with CD8 and 4-1BB sequences, respectively. All CAR cDNAs were cloned in bidirectional lentiviral vectors kindly provided by L. Naldini (San Raffaele-Telethon Institute for Gene Therapy), in which expression of green fluorescent protein (GFP) marker gene was substituted with truncated nerve growth factor receptor devoid of the intracellular signaling domain (ΔNGFR) *(71)*. Briefly, CAR constructs were placed under the direct control of the human

509 phosphoglycerate kinase promoter (PGK) in place of the ΔNGFR marker gene, whereas ΔNGFR was
510 substituted to GFP under the control of a minimal core promoter derived from the cytomegalovirus
511 (minCMV). Viral supernatants were produced in 293T packaging cells.
512
513 **In vitro functional assays**
514 CAR T cells were co-cultured with target cells at different effector:target (E:T) ratios in RPMI-1640
515 fully supplemented in the absence of cytokines. After 24 hours, supernatants were collected and
516 analyzed with the LEGENDplex bead-based cytokine immunoassay (BioLegend, 740724). After 4
517 days (tumors) or 3 days (primary keratinocytes), surviving cells were counted using Flow-Count
518 Fluorospheres (Beckman Coulter, 7547053) and analyzed by flow cytometry. T cells that were
519 untransduced or transduced with an irrelevant CAR (19.28ζ) were used as control. Elimination index
520 was calculated as follows: 1 – (number of residual target cells with experimental CAR T cells /
521 number of residual target cells with control T cells). In co-culture assays addressing the combination
522 of CAR T cells with specific supplements (2DG 4mM 48 hours, Sigma-Aldrich, D6134; Mannose
523 1mM 48 hours, Sigma-Aldrich, 415537; Glucose 1mM 48 hours, Sigma-Aldrich, G8270; 2FDG
524 4mM 48 hours, Sigma-Aldrich, F506; Tunicamycin 100 ng/ml 48 hours, Sigma-Aldrich, 11089-65-
525 9), target cells were exposed to treatments before wash-out and co-culture with CAR T cells. In co-
526 treatment experiments, as specified in figure legends, treatment was not washed-out and the assay
527 took place in its presence. For transcriptional activation studies, CAR^+ Jurkat TPR cells were co-
528 cultured with target cells at 1:1 ratio and reporter gene activation was assessed using CytoFLEX
529 (Beckman Coulter).
530 Lactate production was assessed using the Lactate-Glo assay kit (Promega, J5021) per
531 manufacturer's instructions. Toxicity of 2DG toward hematopoietic compartment was tested by
532 exposing buffy coat cells to 4mM 2DG-supplemented X-VIVO media (Lonza, BE02-054Q) with 2%
533 human serum (Euroclone, ECS0219D), IL-2 (300 IU/mL; Chiron Therapeutics), IL-21 (10 ng/ml;
534 Peprotech, 200-21) and IL-15 (5 ng/mL; Peprotech) for 18 hours. For flow cytometry-based 2-(N-(7-

Nitrobenz-2-oxa-1,3-diazol-4-yl)Amino)-2-Deoxyglucose (2NBDG, Invitrogen, 11569116) uptake assay, cells were incubated with 100μM 2NBDG for 2 hours before measuring fluorescence by flow cytometry.

Mouse experiments

All experiments were approved by the Institutional Animal Care and Use Committee (IACUC) of IRCCS San Raffaele Scientific Institute and by the Italian Governmental Health Institute. Female or male 6 to 9-week-old NOD.Cg-Prkdcscid Il2rgtm1Wjl (NSG) mice (Charles River Laboratories) were kept in a specific-pathogen-free (SPF) facility within individually ventilated cages. For end-point experiments comprising luciferase (Luc^+) T3M-4 pancreatic cancer cells and prophylactic treatment with 2DG prior to CAR T cell therapy, we employed a high and low tumor burden settings. In both settings $0.1x10^6$ tumor cells were injected orthotopically after mice were anesthetized with inhaled isoflurane and oxygen. In high tumor burden experiments, mice were injected intraperitoneally (i.p.) with 500 mg/kg 2DG (Sigma-Aldrich, D6134) on day 6 and 7 after tumor engraftment, before receiving $5x10^6$ CAR T cells intravenously (i.v.). In low tumor burden experiments, mice were treated with 500 mg/kg 2DG on day 2 and day 3 before receiving $10x10^6$ CAR T cells. Tumor growth was monitored by bioluminescence assay using the QUANTI-Luc detection reagent (InvivoGen, rep-qlc1) and expressed as relative light units (RLUs). Mice were euthanized at RLU $\geq 10^6$ in control groups. At euthanasia, tumor masses were retrieved, dissociated using gentleMACS (Miltenyi Biotec, 130-093-235) and tumor dissociation reagents (Miltenyi Biotec, 130-095-929) and analyzed by flow cytometry. For survival experiments with Luc^+ T3M-4 tumors, $0.1x10^6$ tumor cells were injected i.p. and treated with $6.5x10^6$ CAR T cells on day 7. Mice were euthanized at RLU $\geq 10^6$ or when showing signs of discomfort. For survival experiments with Luc^+ BxPC3 pancreatic cancer cells, $0.5x10^6$ tumor cells were injected i.p. and treated with $3x10^6$ CAR T cells on day 7. Mice were euthanized at RLU $\geq 10^6$ or when showing signs of discomfort. For ovarian cancer models using Luc^+ IGROV-1 cells, $0.3x10^6$ tumor cells were injected subcutaneously and

561 treated with $4.5x10^6$ CAR T cells on day 7 *(26)*. For bladder cancer models using Luc^+ 5637 cells,
562 $1x10^6$ tumor cells were injected subcutaneously and treated with $4x10^6$ CAR T cells on day 14. In
563 experiments using IGROV-1 and 5637 tumors, mice received tumor rechallenge on day 19 and 20
564 respectively and were euthanized at RLU $\geq 10^4$ or when showing signs of discomfort. In all
565 experiments comprising the prolonged co-treatment with 2DG, mice received 2DG i.p. at day -1 and
566 0 from CAR T and every day after, with repetitive cycles of 5 days followed by 2-day treatment wash-
567 out.
568
569 **Statistical Analysis**
570 Raw, individual-level data are presented in data file S1. All data are presented as mean ± s.e.m.
571 Statistical analysis was performed on GraphPad Prism 8 software; SPICE software was used for
572 analysis of inhibitory receptors co-expression. Datasets were analyzed with paired or unpaired
573 Student's t-test, one-way or two-way ANOVA and the Log-rank Mantel–Cox tests, depending on the
574 experimental design. Appropriate statistical tests were used as described in the figure legends.
575 Biological replicates are indicated in figure legends as "independent donors", technical replicates are
576 indicated as "independent samples". Differences with a P value < 0.05 were considered statistically
577 significant.
578

Supplementary Materials

Material and Methods

Fig. S1 to S13

Data file S1

583 **References**

584 1. C. J. Turtle, L.-A. Hanafi, C. Berger, M. Hudecek, B. Pender, E. Robinson, R. Hawkins, C. Chaney,
585 S. Cherian, X. Chen, L. Soma, B. Wood, D. Li, S. Heimfeld, S. R. Riddell, D. G. Maloney,
586 Immunotherapy of non-Hodgkin's lymphoma with a defined ratio of CD8+ and CD4+ CD19-specific
587 chimeric antigen receptor-modified T cells, *Sci Transl Med* **8**, 355ra116 (2016).

588 2. S. J. Schuster, J. Svoboda, E. A. Chong, S. D. Nasta, A. R. Mato, Ö. Anak, J. L. Brogdon, I.
589 Pruteanu-Malinici, V. Bhoj, D. Landsburg, M. Wasik, B. L. Levine, S. F. Lacey, J. J. Melenhorst, D.
590 L. Porter, C. H. June, Chimeric Antigen Receptor T Cells in Refractory B-Cell Lymphomas, *N Engl*
591 *J Med* **377**, 2545–2554 (2017).

592 3. J. H. Park, I. Rivière, M. Gonen, X. Wang, B. Sénéchal, K. J. Curran, C. Sauter, Y. Wang, B.
593 Santomasso, E. Mead, M. Roshal, P. Maslak, M. Davila, R. J. Brentjens, M. Sadelain, Long-Term
594 Follow-up of CD19 CAR Therapy in Acute Lymphoblastic Leukemia, *N Engl J Med* **378**, 449–459
595 (2018).

596 4. S. L. Maude, T. W. Laetsch, J. Buechner, S. Rives, M. Boyer, H. Bittencourt, P. Bader, M. R.
597 Verneris, H. E. Stefanski, G. D. Myers, M. Qayed, B. De Moerloose, H. Hiramatsu, K. Schlis, K. L.
598 Davis, P. L. Martin, E. R. Nemecek, G. A. Yanik, C. Peters, A. Baruchel, N. Boissel, F. Mechinaud,
599 A. Balduzzi, J. Krueger, C. H. June, B. L. Levine, P. Wood, T. Taran, M. Leung, K. T. Mueller, Y.
600 Zhang, K. Sen, D. Lebwohl, M. A. Pulsipher, S. A. Grupp, Tisagenlecleucel in Children and Young
601 Adults with B-Cell Lymphoblastic Leukemia, *N Engl J Med* **378**, 439–448 (2018).

602 5. R. G. Majzner, C. L. Mackall, Clinical lessons learned from the first leg of the CAR T cell journey,
603 *Nat Med* **25**, 1341–1355 (2019).

6. W. Xiong, Y. Chen, X. Kang, Z. Chen, P. Zheng, Y.-H. Hsu, J. H. Jang, L. Qin, H. Liu, G. Dotti, D. Liu, Immunological Synapse Predicts Effectiveness of Chimeric Antigen Receptor Cells, *Mol Ther* **26**, 963–975 (2018).

7. C. R. Monks, B. A. Freiberg, H. Kupfer, N. Sciaky, A. Kupfer, Three-dimensional segregation of supramolecular activation clusters in T cells, *Nature* **395**, 82–86 (1998).

8. A. Grakoui, S. K. Bromley, C. Sumen, M. M. Davis, A. S. Shaw, P. M. Allen, M. L. Dustin, The immunological synapse: a molecular machine controlling T cell activation, *Science* **285**, 221–227 (1999).

9. M. Mukherjee, E. M. Mace, A. F. Carisey, N. Ahmed, J. S. Orange, Quantitative Imaging Approaches to Study the CAR Immunological Synapse, *Mol Ther* **25**, 1757–1768 (2017).

10. R. G. Majzner, S. P. Rietberg, E. Sotillo, R. Dong, V. T. Vachharajani, L. Labanieh, J. H. Myklebust, M. Kadapakkam, E. W. Weber, A. M. Tousley, R. M. Richards, S. Heitzeneder, S. M. Nguyen, V. Wiebking, J. Theruvath, R. C. Lynn, P. Xu, A. R. Dunn, R. D. Vale, C. L. Mackall, Tuning the Antigen Density Requirement for CAR T-cell Activity, *Cancer Discov* **10**, 702–723 (2020).

11. F. Schwarz, M. Aebi, Mechanisms and principles of N-linked protein glycosylation, *Curr Opin Struct Biol* **21**, 576–582 (2011).

12. C. Reily, T. J. Stewart, M. B. Renfrow, J. Novak, Glycosylation in health and disease, *Nat Rev Nephrol* **15**, 346–366 (2019).

13. M. Bartish, S. V. Del Rincón, C. E. Rudd, H. U. Saragovi, Aiming for the Sweet Spot: Glyco-Immune Checkpoints and γδ T Cells in Targeted Immunotherapy, *Front Immunol* **11**, 564499 (2020).

14. C. Jandus, K. F. Boligan, O. Chijioke, H. Liu, M. Dahlhaus, T. Démoulins, C. Schneider, M. Wehrli, R. E. Hunger, G. M. Baerlocher, H.-U. Simon, P. Romero, C. Münz, S. von Gunten, Interactions between Siglec-7/9 receptors and ligands influence NK cell-dependent tumor immunosurveillance, *J Clin Invest* **124**, 1810–1820 (2014).

15. R. Beatson, V. Tajadura-Ortega, D. Achkova, G. Picco, T.-D. Tsourouktsoglou, S. Klausing, M. Hillier, J. Maher, T. Noll, P. R. Crocker, J. Taylor-Papadimitriou, J. M. Burchell, The mucin MUC1 modulates the tumor immunological microenvironment through engagement of the lectin Siglec-9, *Nat Immunol* **17**, 1273–1281 (2016).

16. A. D. Posey, R. D. Schwab, A. C. Boesteanu, C. Steentoft, U. Mandel, B. Engels, J. D. Stone, T. D. Madsen, K. Schreiber, K. M. Haines, A. P. Cogdill, T. J. Chen, D. Song, J. Scholler, D. M. Kranz, M. D. Feldman, R. Young, B. Keith, H. Schreiber, H. Clausen, L. A. Johnson, C. H. June, Engineered CAR T Cells Targeting the Cancer-Associated Tn-Glycoform of the Membrane Mucin MUC1 Control Adenocarcinoma, *Immunity* **44**, 1444–1454 (2016).

17. S. S. Pinho, C. A. Reis, Glycosylation in cancer: mechanisms and clinical implications, *Nat Rev Cancer* **15**, 540–555 (2015).

18. M. Shoreibah, G. S. Perng, B. Adler, J. Weinstein, R. Basu, R. Cupples, D. Wen, J. K. Browne, P. Buckhaults, N. Fregien, M. Pierce, Isolation, characterization, and expression of a cDNA encoding N-acetylglucosaminyltransferase V, *J Biol Chem* **268**, 15381–15385 (1993).

19. R. Kang, H. Saito, Y. Ihara, E. Miyoshi, N. Koyama, Y. Sheng, N. Taniguchi, Transcriptional regulation of the N-acetylglucosaminyltransferase V gene in human bile duct carcinoma cells (HuCC-T1) is mediated by Ets-1, *J Biol Chem* **271**, 26706–26712 (1996).

20. M. Granovsky, J. Fata, J. Pawling, W. J. Muller, R. Khokha, J. W. Dennis, Suppression of tumor growth and metastasis in Mgat5-deficient mice, *Nat Med* **6**, 306–312 (2000).

21. J. W. Dennis, S. Laferté, C. Waghorne, M. L. Breitman, R. S. Kerbel, Beta 1-6 branching of Asn-linked oligosaccharides is directly associated with metastasis, *Science* **236**, 582–585 (1987).

22. B. Fernandes, U. Sagman, M. Auger, M. Demetrio, J. W. Dennis, Beta 1-6 branched oligosaccharides as a marker of tumor progression in human breast and colon neoplasia, *Cancer Res* **51**, 718–723 (1991).

23. W. K. Seelentag, W. P. Li, S. F. Schmitz, U. Metzger, P. Aeberhard, P. U. Heitz, J. Roth, Prognostic value of beta1,6-branched oligosaccharides in human colorectal carcinoma, *Cancer Res* **58**, 5559–5564 (1998).

24. M. Casucci, B. Nicolis di Robilant, L. Falcone, B. Camisa, M. Norelli, P. Genovese, B. Gentner, F. Gullotta, M. Ponzoni, M. Bernardi, M. Marcatti, A. Saudemont, C. Bordignon, B. Savoldo, F. Ciceri, L. Naldini, G. Dotti, C. Bonini, A. Bondanza, CD44v6-targeted T cells mediate potent antitumor effects against acute myeloid leukemia and multiple myeloma, *Blood* **122**, 3461–3472 (2013).

25. M. Casucci, L. Falcone, B. Camisa, M. Norelli, S. Porcellini, A. Stornaiuolo, F. Ciceri, C. Traversari, C. Bordignon, C. Bonini, A. Bondanza, Extracellular NGFR Spacers Allow Efficient Tracking and Enrichment of Fully Functional CAR-T Cells Co-Expressing a Suicide Gene, *Front Immunol* **9**, 507 (2018).

26. S. Porcellini, C. Asperti, S. Corna, E. Cicoria, V. Valtolina, A. Stornaiuolo, B. Valentinis, C. Bordignon, C. Traversari, CAR T Cells Redirected to CD44v6 Control Tumor Growth in Lung and Ovary Adenocarcinoma Bearing Mice, *Front Immunol* **11**, 99 (2020).

27. F. C. Thistlethwaite, D. E. Gilham, R. D. Guest, D. G. Rothwell, M. Pillai, D. J. Burt, A. J. Byatte, N. Kirillova, J. W. Valle, S. K. Sharma, K. A. Chester, N. B. Westwood, S. E. R. Halford, S. Nabarro, S. Wan, E. Austin, R. E. Hawkins, The clinical efficacy of first-generation carcinoembryonic antigen

(CEACAM5)-specific CAR T cells is limited by poor persistence and transient pre-conditioning-dependent respiratory toxicity, *Cancer Immunol Immunother* **66**, 1425–1436 (2017).

28. C. Zhang, Z. Wang, Z. Yang, M. Wang, S. Li, Y. Li, R. Zhang, Z. Xiong, Z. Wei, J. Shen, Y. Luo, Q. Zhang, L. Liu, H. Qin, W. Liu, F. Wu, W. Chen, F. Pan, X. Zhang, P. Bie, H. Liang, G. Pecher, C. Qian, Phase I Escalating-Dose Trial of CAR-T Therapy Targeting CEA+ Metastatic Colorectal Cancers, *Mol Ther* **25**, 1248–1258 (2017).

29. S. C. Katz, J. Hardaway, E. Prince, P. Guha, M. Cunetta, A. Moody, L. J. Wang, V. Armenio, N. J. Espat, R. P. Junghans, HITM-SIR: phase Ib trial of intraarterial chimeric antigen receptor T-cell therapy and selective internal radiation therapy for CEA+ liver metastases, *Cancer Gene Ther* **27**, 341–355 (2020).

30. E. Lisowska, The role of glycosylation in protein antigenic properties, *Cell Mol Life Sci* **59**, 445–455 (2002).

31. K. H. Heider, M. Sproll, S. Susani, E. Patzelt, P. Beaumier, E. Ostermann, H. Ahorn, G. R. Adolf, Characterization of a high-affinity monoclonal antibody specific for CD44v6 as candidate for immunotherapy of squamous cell carcinomas, *Cancer Immunol Immunother* **43**, 245–253 (1996).

32. K. Munk, E. Pritzer, E. Kretzschmar, B. Gutte, W. Garten, H. D. Klenk, Carbohydrate masking of an antigenic epitope of influenza virus haemagglutinin independent of oligosaccharide size, *Glycobiology* **2**, 233–240 (1992).

33. D. I. Spencer, S. Missailidis, G. Denton, A. Murray, K. Brady, C. I. Matteis, M. S. Searle, S. J. Tendler, M. R. Price, Structure/activity studies of the anti-MUC1 monoclonal antibody C595 and synthetic MUC1 mucin-core-related peptides and glycopeptides, *Biospectroscopy* **5**, 79–91 (1999).

34. H.-H. Lee, Y.-N. Wang, W. Xia, C.-H. Chen, K.-M. Rau, L. Ye, Y. Wei, C.-K. Chou, S.-C. Wang, M. Yan, C.-Y. Tu, T.-C. Hsia, S.-F. Chiang, K. S. C. Chao, I. I. Wistuba, J. L. Hsu, G. N. Hortobagyi,

694 M.-C. Hung, Removal of N-Linked Glycosylation Enhances PD-L1 Detection and Predicts Anti-PD-
695 1/PD-L1 Therapeutic Efficacy, *Cancer Cell* **36**, 168-178.e4 (2019).

696 35. M. G. Vander Heiden, L. C. Cantley, C. B. Thompson, Understanding the Warburg effect: the
697 metabolic requirements of cell proliferation, *Science* **324**, 1029–1033 (2009).

698 36. M. Stein, H. Lin, C. Jeyamohan, D. Dvorzhinski, M. Gounder, K. Bray, S. Eddy, S. Goodin, E.
699 White, R. S. Dipaola, Targeting tumor metabolism with 2-deoxyglucose in patients with castrate-
700 resistant prostate cancer and advanced malignancies, *Prostate* **70**, 1388–1394 (2010).

701 37. E. Cerami, J. Gao, U. Dogrusoz, B. E. Gross, S. O. Sumer, B. A. Aksoy, A. Jacobsen, C. J. Byrne,
702 M. L. Heuer, E. Larsson, Y. Antipin, B. Reva, A. P. Goldberg, C. Sander, N. Schultz, The cBio cancer
703 genomics portal: an open platform for exploring multidimensional cancer genomics data, *Cancer*
704 *Discov* **2**, 401–404 (2012).

705 38. J. Gao, B. A. Aksoy, U. Dogrusoz, G. Dresdner, B. Gross, S. O. Sumer, Y. Sun, A. Jacobsen, R.
706 Sinha, E. Larsson, E. Cerami, C. Sander, N. Schultz, Integrative analysis of complex cancer genomics
707 and clinical profiles using the cBioPortal, *Sci Signal* **6**, pl1 (2013).

708 39. A. Subramanian, P. Tamayo, V. K. Mootha, S. Mukherjee, B. L. Ebert, M. A. Gillette, A.
709 Paulovich, S. L. Pomeroy, T. R. Golub, E. S. Lander, J. P. Mesirov, Gene set enrichment analysis: a
710 knowledge-based approach for interpreting genome-wide expression profiles, *Proc Natl Acad Sci U*
711 *S A* **102**, 15545–15550 (2005).

712 40. H. Ponta, L. Sherman, P. A. Herrlich, CD44: from adhesion molecules to signalling regulators,
713 *Nat Rev Mol Cell Biol* **4**, 33–45 (2003).

714 41. A. Bondanza, V. Valtolina, Z. Magnani, M. Ponzoni, K. Fleischhauer, M. Bonyhadi, C.
715 Traversari, F. Sanvito, S. Toma, M. Radrizzani, S. La Seta-Catamancio, F. Ciceri, C. Bordignon, C.

716 Bonini, Suicide gene therapy of graft-versus-host disease induced by central memory human T
717 lymphocytes, *Blood* **107**, 1828–1836 (2006).

718 42. S. Kaneko, S. Mastaglio, A. Bondanza, M. Ponzoni, F. Sanvito, L. Aldrighetti, M. Radrizzani, S.
719 La Seta-Catamancio, E. Provasi, A. Mondino, T. Nagasawa, K. Fleischhauer, V. Russo, C. Traversari,
720 F. Ciceri, C. Bordignon, C. Bonini, IL-7 and IL-15 allow the generation of suicide gene-modified
721 alloreactive self-renewing central memory human T lymphocytes, *Blood* **113**, 1006–1015 (2009).

722 43. S. Arcangeli, L. Falcone, B. Camisa, F. De Girardi, M. Biondi, F. Giglio, F. Ciceri, C. Bonini, A.
723 Bondanza, M. Casucci, Next-Generation Manufacturing Protocols Enriching TSCM CAR T Cells
724 Can Overcome Disease-Specific T Cell Defects in Cancer Patients, *Front Immunol* **11**, 1217 (2020).

725 44. A. N. Mentlik, K. B. Sanborn, E. L. Holzbaur, J. S. Orange, Rapid lytic granule convergence to
726 the MTOC in natural killer cells is dependent on dynein but not cytolytic commitment, *Mol Biol Cell*
727 **21**, 2241–2256 (2010).

728 45. M. Hegde, M. Mukherjee, Z. Grada, A. Pignata, D. Landi, S. A. Navai, A. Wakefield, K. Fousek,
729 K. Bielamowicz, K. K. H. Chow, V. S. Brawley, T. T. Byrd, S. Krebs, S. Gottschalk, W. S. Wels, M.
730 L. Baker, G. Dotti, M. Mamonkin, M. K. Brenner, J. S. Orange, N. Ahmed, Tandem CAR T cells
731 targeting HER2 and IL13Rα2 mitigate tumor antigen escape, *J Clin Invest* **126**, 3036–3052 (2016).

732 46. S. Jutz, J. Leitner, K. Schmetterer, I. Doel-Perez, O. Majdic, K. Grabmeier-Pfistershammer, W.
733 Paster, J. B. Huppa, P. Steinberger, Assessment of costimulation and coinhibition in a triple parameter
734 T cell reporter line: Simultaneous measurement of NF-κB, NFAT and AP-1, *J Immunol Methods* **430**,
735 10–20 (2016).

736 47. D. Zhang, J. Li, F. Wang, J. Hu, S. Wang, Y. Sun, 2-Deoxy-D-glucose targeting of glucose
737 metabolism in cancer cells as a potential therapy, *Cancer Lett* **355**, 176–183 (2014).

738 48. M. Kurtoglu, N. Gao, J. Shang, J. C. Maher, M. A. Lehrman, M. Wangpaichitr, N. Savaraj, A. N.
739 Lane, T. J. Lampidis, Under normoxia, 2-deoxy-D-glucose elicits cell death in select tumor types not
740 by inhibition of glycolysis but by interfering with N-linked glycosylation, *Mol Cancer Ther* **6**, 3049–
741 3058 (2007).

742 49. L. Falcone, M. Casucci, Exploiting Secreted Luciferases to Monitor Tumor Progression In Vivo,
743 *Methods Mol Biol* **1393**, 105–111 (2016).

744 50. C.-W. Li, S.-O. Lim, E. M. Chung, Y.-S. Kim, A. H. Park, J. Yao, J.-H. Cha, W. Xia, L.-C. Chan,
745 T. Kim, S.-S. Chang, H.-H. Lee, C.-K. Chou, Y.-L. Liu, H.-C. Yeh, E. P. Perillo, A. K. Dunn, C.-W.
746 Kuo, K.-H. Khoo, J. L. Hsu, Y. Wu, J.-M. Hsu, H. Yamaguchi, T.-H. Huang, A. A. Sahin, G. N.
747 Hortobagyi, S. S. Yoo, M.-C. Hung, Eradication of Triple-Negative Breast Cancer Cells by Targeting
748 Glycosylated PD-L1, *Cancer Cell* **33**, 187-201.e10 (2018).

749 51. C.-W. Li, S.-O. Lim, W. Xia, H.-H. Lee, L.-C. Chan, C.-W. Kuo, K.-H. Khoo, S.-S. Chang, J.-H.
750 Cha, T. Kim, J. L. Hsu, Y. Wu, J.-M. Hsu, H. Yamaguchi, Q. Ding, Y. Wang, J. Yao, C.-C. Lee, H.-
751 J. Wu, A. A. Sahin, J. P. Allison, D. Yu, G. N. Hortobagyi, M.-C. Hung, Glycosylation and
752 stabilization of programmed death ligand-1 suppresses T-cell activity, *Nat Commun* **7**, 12632 (2016).

753 52. R. Magistroni, A. Boletta, Defective glycolysis and the use of 2-deoxy-D-glucose in polycystic
754 kidney disease: from animal models to humans, *J Nephrol* **30**, 511–519 (2017).

755 53. K. Yamada, M. Saito, H. Matsuoka, N. Inagaki, A real-time method of imaging glucose uptake
756 in single, living mammalian cells, *Nat Protoc* **2**, 753–762 (2007).

757 54. M. Sukumar, J. Liu, Y. Ji, M. Subramanian, J. G. Crompton, Z. Yu, R. Roychoudhuri, D. C.
758 Palmer, P. Muranski, E. D. Karoly, R. P. Mohney, C. A. Klebanoff, A. Lal, T. Finkel, N. P. Restifo,
759 L. Gattinoni, Inhibiting glycolytic metabolism enhances CD8+ T cell memory and antitumor
760 function, *J Clin Invest* **123**, 4479–4488 (2013).

761 55. Z. Yang, J. Peltonen, S. Kaski, Scalable optimization of neighbor embedding for visualization,
762 *Icml* **28**, 786–794 (2013).

763 56. M. Noviello, F. Manfredi, E. Ruggiero, T. Perini, G. Oliveira, F. Cortesi, P. De Simone, C.
764 Toffalori, V. Gambacorta, R. Greco, J. Peccatori, M. Casucci, G. Casorati, P. Dellabona, M.
765 Onozawa, T. Teshima, M. Griffioen, C. J. M. Halkes, J. H. F. Falkenburg, F. Stölzel, H. Altmann, M.
766 Bornhäuser, M. Waterhouse, R. Zeiser, J. Finke, N. Cieri, A. Bondanza, L. Vago, F. Ciceri, C. Bonini,
767 Bone marrow central memory and memory stem T-cell exhaustion in AML patients relapsing after
768 HSCT, *Nat Commun* **10**, 1065 (2019).

769 57. F. Manfredi, D. Abbati, B. C. Cianciotti, L. Stasi, A. Potenza, E. Ruggiero, Z. Magnani, E.
770 Carnevale, M. Doglio, M. Noviello, E. Tassi, C. Balestrieri, S. Buonanno, F. Clemente, C. De Lalla,
771 M. P. Protti, A. Mondino, G. Casorati, P. Dellabona, C. Bonini, Flow cytometry data mining by
772 cytoChain identifies determinants of exhaustion and stemness in TCR-engineered T cells, *Eur J*
773 *Immunol* (2021), doi:10.1002/eji.202049103.

774 58. S. J. Davis, P. A. van der Merwe, The kinetic-segregation model: TCR triggering and beyond,
775 *Nat Immunol* **7**, 803–809 (2006).

776 59. J. Li, N. J. Stagg, J. Johnston, M. J. Harris, S. A. Menzies, D. DiCara, V. Clark, M. Hristopoulos,
777 R. Cook, D. Slaga, R. Nakamura, L. McCarty, S. Sukumaran, E. Luis, Z. Ye, T. D. Wu, T. Sumiyoshi,
778 D. Danilenko, G. Y. Lee, K. Totpal, D. Ellerman, I. Hötzel, J. R. James, T. T. Junttila, Membrane-
779 Proximal Epitope Facilitates Efficient T Cell Synapse Formation by Anti-FcRH5/CD3 and Is a
780 Requirement for Myeloma Cell Killing, *Cancer Cell* **31**, 383–395 (2017).

781 60. R. Grosser, L. Cherkassky, N. Chintala, P. S. Adusumilli, Combination Immunotherapy with
782 CAR T Cells and Checkpoint Blockade for the Treatment of Solid Tumors, *Cancer Cell* **36**, 471–482
783 (2019).

784 61. R. C. Lynn, E. W. Weber, E. Sotillo, D. Gennert, P. Xu, Z. Good, H. Anbunathan, J. Lattin, R.
785 Jones, V. Tieu, S. Nagaraja, J. Granja, C. F. A. de Bourcy, R. Majzner, A. T. Satpathy, S. R. Quake,
786 M. Monje, H. Y. Chang, C. L. Mackall, c-Jun overexpression in CAR T cells induces exhaustion
787 resistance, *Nature* **576**, 293–300 (2019).

788 62. D. Singh, A. K. Banerji, B. S. Dwarakanath, R. P. Tripathi, J. P. Gupta, T. L. Mathew, T.
789 Ravindranath, V. Jain, Optimizing cancer radiotherapy with 2-deoxy-d-glucose dose escalation
790 studies in patients with glioblastoma multiforme, *Strahlenther Onkol* **181**, 507–514 (2005).

791 63. L. E. Raez, K. Papadopoulos, A. D. Ricart, E. G. Chiorean, R. S. Dipaola, M. N. Stein, C. M.
792 Rocha Lima, J. J. Schlesselman, K. Tolba, V. K. Langmuir, S. Kroll, D. T. Jung, M. Kurtoglu, J.
793 Rosenblatt, T. J. Lampidis, A phase I dose-escalation trial of 2-deoxy-D-glucose alone or combined
794 with docetaxel in patients with advanced solid tumors, *Cancer Chemother Pharmacol* **71**, 523–530
795 (2013).

796 64. E. A. Mesri, T. J. Lampidis, 2-Deoxy-d-glucose exploits increased glucose metabolism in cancer
797 and viral-infected cells: Relevance to its use in India against SARS-CoV-2, *IUBMB Life* **73**, 1198–
798 1204 (2021).

799 65. H. Xi, M. Kurtoglu, T. J. Lampidis, The wonders of 2-deoxy-D-glucose, *IUBMB Life* **66**, 110–
800 121 (2014).

801 66. M. D. Kornberg, The immunologic Warburg effect: Evidence and therapeutic opportunities in
802 autoimmunity, *Wiley Interdiscip Rev Syst Biol Med* **12**, e1486 (2020).

803 67. C.-H. Chang, J. D. Curtis, L. B. Maggi, B. Faubert, A. V. Villarino, D. O'Sullivan, S. C.-C.
804 Huang, G. J. W. van der Windt, J. Blagih, J. Qiu, J. D. Weber, E. J. Pearce, R. G. Jones, E. L. Pearce,
805 Posttranscriptional control of T cell effector function by aerobic glycolysis, *Cell* **153**, 1239–1251
806 (2013).

807 68. J. A. Fraietta, S. F. Lacey, E. J. Orlando, I. Pruteanu-Malinici, M. Gohil, S. Lundh, A. C.
808 Boesteanu, Y. Wang, R. S. O'Connor, W.-T. Hwang, E. Pequignot, D. E. Ambrose, C. Zhang, N.
809 Wilcox, F. Bedoya, C. Dorfmeier, F. Chen, L. Tian, H. Parakandi, M. Gupta, R. M. Young, F. B.
810 Johnson, I. Kulikovskaya, L. Liu, J. Xu, S. H. Kassim, M. M. Davis, B. L. Levine, N. V. Frey, D. L.
811 Siegel, A. C. Huang, E. J. Wherry, H. Bitter, J. L. Brogdon, D. L. Porter, C. H. June, J. J. Melenhorst,
812 Determinants of response and resistance to CD19 chimeric antigen receptor (CAR) T cell therapy of
813 chronic lymphocytic leukemia, *Nat Med* **24**, 563–571 (2018).

814 69. Q. Deng, G. Han, N. Puebla-Osorio, M. C. J. Ma, P. Strati, B. Chasen, E. Dai, M. Dang, N. Jain,
815 H. Yang, Y. Wang, S. Zhang, R. Wang, R. Chen, J. Showell, S. Ghosh, S. Patchva, Q. Zhang, R. Sun,
816 F. Hagemeister, L. Fayad, F. Samaniego, H. C. Lee, L. J. Nastoupil, N. Fowler, R. Eric Davis, J.
817 Westin, S. S. Neelapu, L. Wang, M. R. Green, Characteristics of anti-CD19 CAR T cell infusion
818 products associated with efficacy and toxicity in patients with large B cell lymphomas, *Nat Med* **26**,
819 1878–1887 (2020).

820 70. L. Gattinoni, D. E. Speiser, M. Lichterfeld, C. Bonini, T memory stem cells in health and disease,
821 *Nat Med* **23**, 18–27 (2017).

822 71. B. Savoldo, C. A. Ramos, E. Liu, M. P. Mims, M. J. Keating, G. Carrum, R. T. Kamble, C. M.
823 Bollard, A. P. Gee, Z. Mei, H. Liu, B. Grilley, C. M. Rooney, H. E. Heslop, M. K. Brenner, G. Dotti,
824 CD28 costimulation improves expansion and persistence of chimeric antigen receptor-modified T
825 cells in lymphoma patients, *J Clin Invest* **121**, 1822–1826 (2011).

826 72. M. Amendola, M. A. Venneri, A. Biffi, E. Vigna, L. Naldini, Coordinate dual-gene transgenesis
827 by lentiviral vectors carrying synthetic bidirectional promoters, *Nat Biotechnol* **23**, 108–116 (2005).

828 73. E. D. Amir, K. L. Davis, M. D. Tadmor, E. F. Simonds, J. H. Levine, S. C. Bendall, D. K.
829 Shenfeld, S. Krishnaswamy, G. P. Nolan, D. Pe'er, viSNE enables visualization of high dimensional

single-cell data and reveals phenotypic heterogeneity of leukemia, *Nat Biotechnol* **31**, 545–552 (2013).

74. KEGG PATHWAY: N-Glycan biosynthesis - Reference pathway (available at https://www.genome.jp/kegg-bin/show_pathway?map00510).

75. Z. Tang, B. Kang, C. Li, T. Chen, Z. Zhang, GEPIA2: an enhanced web server for large-scale expression profiling and interactive analysis, *Nucleic Acids Research* **47**, W556–W560 (2019).

Acknowledgements: We thank G. Dotti (University of North Carolina) and H. Abken (University of Cologne) for providing the original CAR constructs, L. Naldini (San Raffaele-Telethon Institute for Gene Therapy) for providing the bidirectional lentiviral backbone and P. Steinberger (University of Vienna) for providing Jurkat triple reporter cells upon material transfer agreement. We acknowledge A. Boletta (IRCCS San Raffaele Scientific Institute) for scientific discussion on 2DG and ALEMBIC (advanced microscopy laboratory; IRCCS San Raffaele Scientific Institute) for technical support. We thank L. Piemonti for kindly providing PT45, A8184 and PaCa44 pancreatic tumor cell lines.

Funding: This work was supported by the Italian Association for Cancer Research (AIRC 5 per Mille Rif. 22737 to M.C. and C.B.), by the Italian Ministry of Health and Alliance Against Cancer (Ricerca Corrente CAR T project: RCR-2019-23669115 to M.C., F.C. and C.B.), by the European Union's Horizon 2020 research and innovation programmed under Grant Agreement No. 733297 (EURE-CART to M.C. and F.C.) and Grant Agreement No. 754658 (CARAMBA to M.C. and F.C.). Moreover, this work was supported by Fondazione Telethon (GGP16252 to A.G.) and by PRIN (PRIN_2015_4CWJH4 to A.G.). E.A. was supported by a FIRC-AIRC fellowship for Italy. **Author contributions:** B.G. designed and performed experiments, analyzed data, interpreted results, and wrote the manuscript. V.M designed and performed experiments, analyzed data, and interpreted results. F.D. performed experiments, analyzed data, and interpreted results. G.M.S. performed genomic and RNAseq data analysis and interpreted results. F.M. performed the BH-SNE analysis. E.A., C.S., B.C., L.F., K.P. and M.B. performed experiments and analyzed data. M.A.M. assisted with figures and summary graphic processing. R.N., F.S. and C.D. performed histopathological analysis. S.A. offered scientific support for experiment design and discussion. A.G., F.C., C.B. and A.B. contributed to scientific discussion and manuscript revision. M.C. designed experiments and interpreted results, wrote the manuscript, and acted as senior author of the study. **Competing interests:** C.B. received research support from Intellia Therapeutics. A.B. is currently an employee of AstraZeneca plc. He contributed to this work until December 2017 when he was an employee of Vita-Salute San Raffaele University. K.P. is currently an employee of AstraZeneca Italy. Her

863 contribution to this work relates to the period 2017-January 2019 when she was an employee of
864 IRCCS San Raffaele Scientific Institute. All other authors declare no competing interests. M.C., B.G.
865 and A.B. are inventors on patent application #PCT/EP2021/061198 submitted by Ospedale San
866 Raffaele (OSR) and Fondazione Centro San Raffaele (FCSR) that covers "Combination of a
867 glycosylation inhibitor with one CAR cell therapy for treating cancer". C. B. and A. B. are inventors
868 on patent # PCT/IT2006/000600 submitted by Ospedale San Raffaele (OSR) that covers "Use of
869 common g-chain cytokines for the visualization, isolation and genetic modification of memory T
870 lymphocytes".
871 **Data and materials availability:** All data associated with this study are in the paper or
872 supplementary materials. All reagents will be made available to members of the research community
873 upon reasonable request after completion of a material transfer agreement. Reagent requests should
874 be directed to M.C. (casucci.monica@hsr.it).
875

Figure Legends

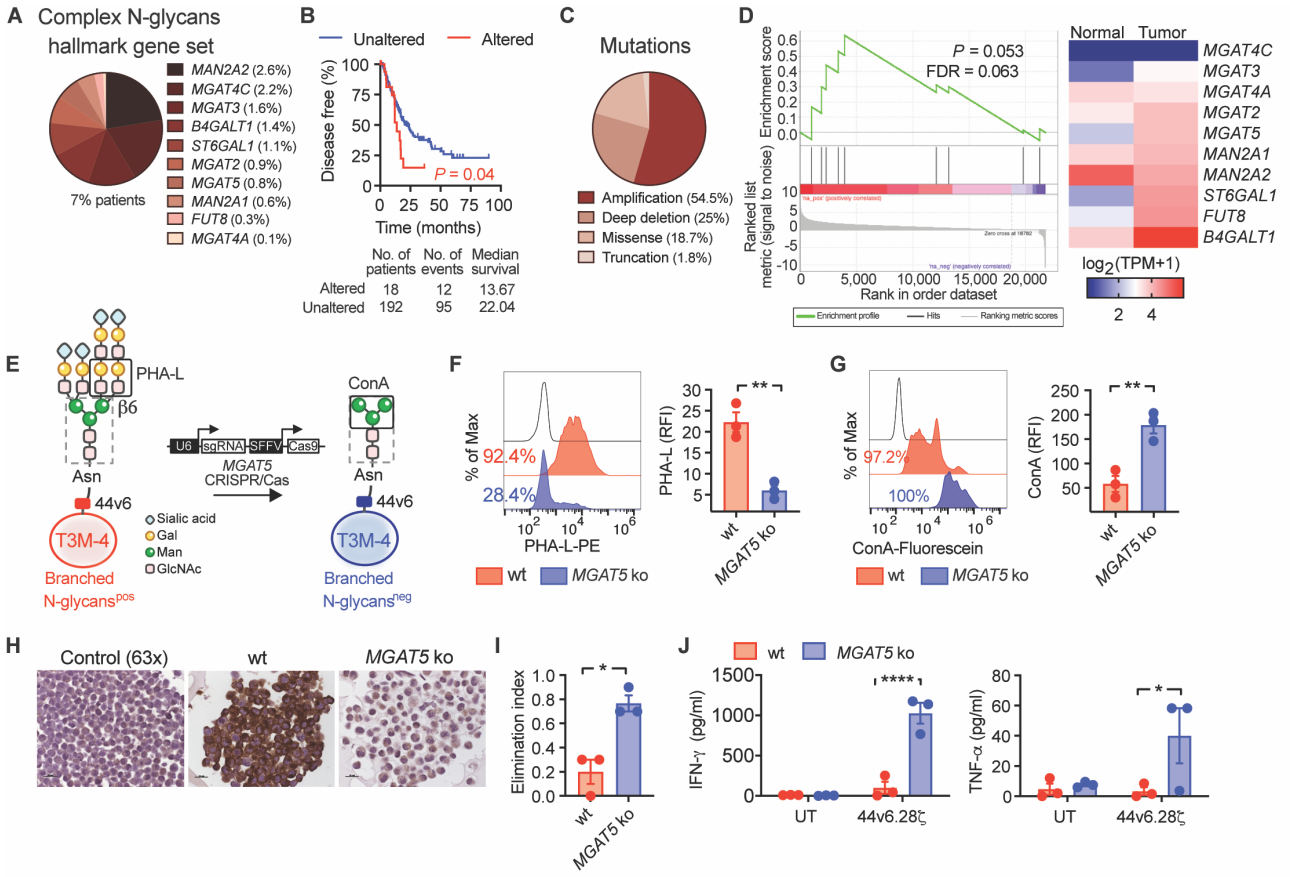

Fig. 1. Branched N-glycans protect pancreatic adenocarcinoma from 44v6.28ζ cells. (**A**) The frequency of patients with pancreatic adenocarcinoma carrying at least one genomic alteration in glycosyltransferases responsible for the synthesis of branched N-glycans was quantified using the cBioportal database (n = 1033). (**B**) A Kaplan-Meier plot comparing disease-free survival rates in patients with unaltered versus altered glycosyltransferases from (**A**) is shown. (**C**) The frequency of mutations types in patients with altered glycosyltransferases is shown (n = 77). (**D**) Left: Pre-ranked GSEA is shown for the expression profile of tumor tissue samples from patients with pancreatic cancer and adjacent normal tissue samples using branched N-glycans glycosyltransferases gene set. Right: A heat map of gene expression is shown. Expression data were retrieved from TCGA and GTEx databases using Gepia2. (**E**) A schematic representation of N-glycans is shown for T3M-4 wild-type (wt) or T3M-4 cells knocked-out for the expression of the glycosyltransferase *MGAT5* (*MGAT5* KO). Phytohemagglutinin-L (PHA-L) and Concanavalin A (ConA) specificities are shown

890 (dark box). The dotted gray box shows core N-glycans. (**F** and **G**) Flow cytometric profiles of PHA-
891 L (**F**) and ConA (**G**) binding to T3M-4 are shown. Left, representative plots showing frequency of
892 positive cells. Negative control is shown in white. Right, relative fluorescence intensity (RFI, $n = 3$
893 independent samples). (**H**) PHA-L binding (brown) to T3M-4 cell-block sections is shown. Control,
894 unstained cells. Scale: 20 μm. (**I**) Target cell killing was measured after T3M-4 cells were co-cultured
895 with 44v6.28ζ at 1:10 effector:target (E:T) ratio. Killing is expressed as elimination index, which was
896 calculated as compared to control T cells (see Methods; $n = 3$ donors). (**J**) IFN-γ and TNF-α
897 production after co-culture of 44v6.28ζ with target cells is shown ($n = 3$ donors). UT, untransduced
898 T cells. *P* values (*$P < 0.05$; **$P < 0.01$; ****$P < 0.0001$) were determined by log-rank Mantel-Cox
899 test (**B**), two-tailed *t*-test (**F**, **G**, **I**) or two-way ANOVA (**J**). Data are presented as mean ± s.e.m.
900

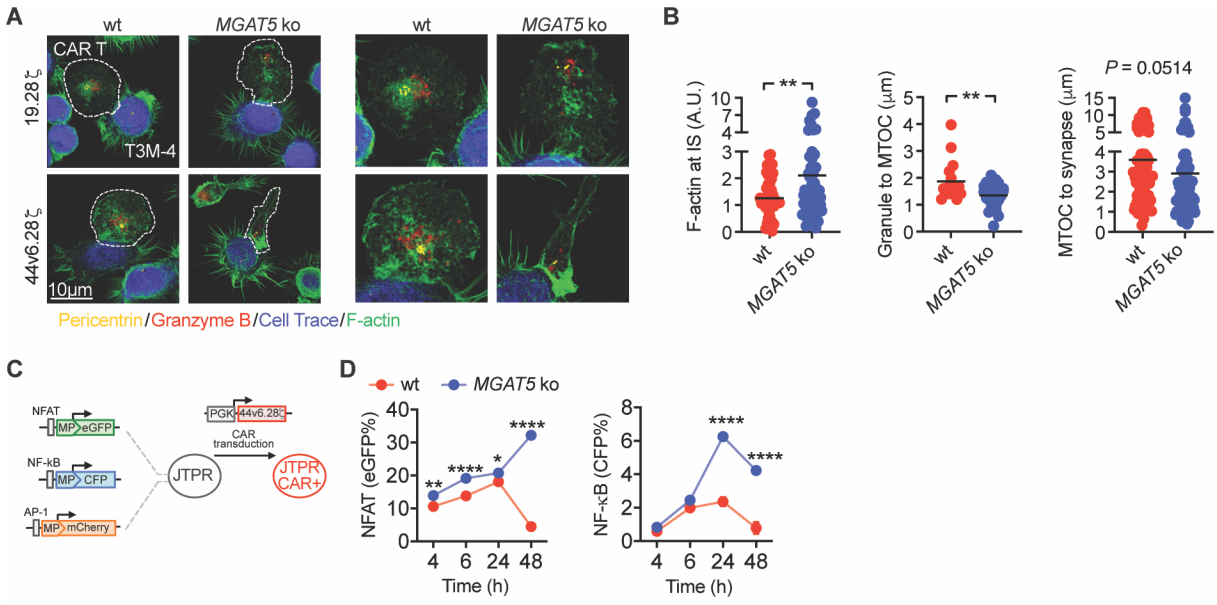

Fig. 2. Removing MGAT5 N-glycan products results in superior immunological synapse quality and improves CAR signaling. (**A**) Left, confocal microscopy images showing conjugation of CAR T cells (dotted line) with target T3M-4 cells. Scale: 10 μm. Right, image magnification onto a representative immunological synapse (IS) showing pericentrin (yellow), F-actin (Phalloidin, green), granzyme B (red), and a target T3M-4 cell (blue). (**B**) Quantification of F-actin accumulation, granzyme lytic granules convergence, and microtubule-organizing-center (MTOC) polarization were quantified from 44v6.28ζ cells engaged in an IS with target T3M-4 cells. Each dot represents one IS quantification from 3 donors of independent experiments (n = 58 for T3M-4 wt; n = 62 for T3M-4 *MGAT5* ko). A.U., arbitrary units. (**C**) Schematic representation of the Jurkat triple reporter (TPR) CAR$^+$ system is shown. Jurkat TPR were transduced with 44v6.28ζ, allowing measurement of CAR-induced activation of transcription factors through the expression of fluorescent proteins. (**D**) Frequency of NFAT and NF-κB activation in 44v6.28ζ$^+$ Jurkat TPR was measured during a time-course stimulation with target T3M-4 cells (n = 3 independent samples). P values (*P < 0.05; ** P < 0.01; ****P < 0.0001) were determined by two-tailed t-test (**B**) or two-way ANOVA (**D**). Data are presented as mean ± s.e.m.

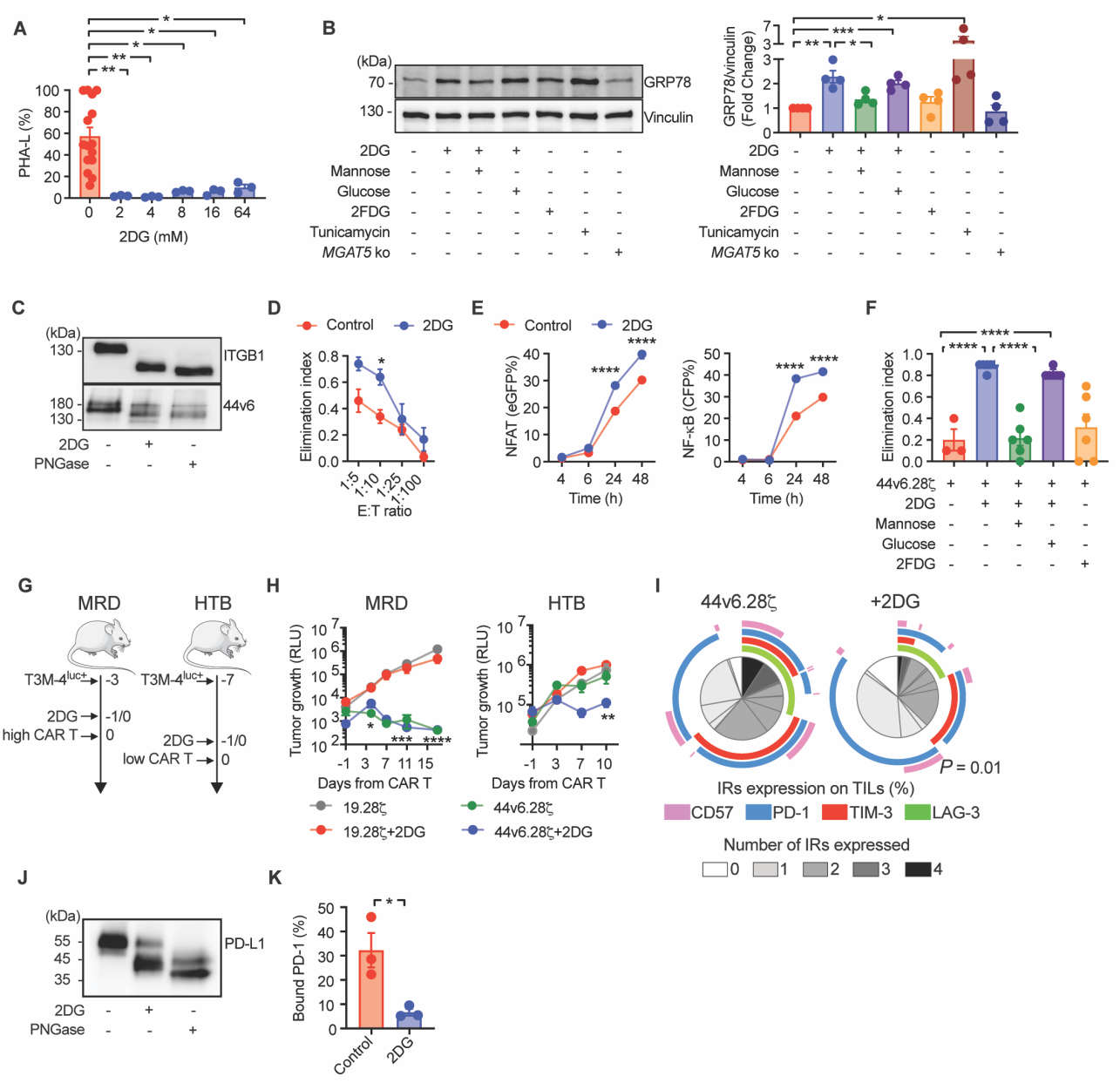

Fig. 3. Prophylactic treatment with 2DG inhibits N-glycosylation and sensitizes pancreatic tumors to 44v6.28ζ cells. (**A**) Frequency of PHA-L binding to T3M-4 cells treated with incremental concentrations of 2DG for 48 hours is shown (n = 3 to 15 independent samples). (**B**) Western blot analysis of T3M-4 lysates shows expression of the ER stress protein GRP78 upon treatment with the indicated drugs. *MGAT5* ko denotes control *MGAT5* knocked-out T3M-4. Left, representative western blot. Right, quantification of GRP78 protein normalized over vinculin from 4 independent experiments. (**C**) Pull down of biotinylated surface proteins from T3M-4 extracellular membrane lysates showing β1 integrin (ITGB1) and CD44v6 molecular weight shifts upon treatment with 2DG

(4mM, 48h) or control PNGase F (representative of three experiments). (**D**) Killing of T3M-4 cells was quantified after co-culture with 44v6.28ζ cells at different effector:target (E:T) ratios (*n* = 5 donors). (**E**) Frequency of NFAT and NF-κB activation was measured in 44v6.28ζ^{+} Jurkat TPR cells during a time-course stimulation with T3M-4 target cells (*n* = 3 independent samples). (**F**) Killing of T3M-4 cells was quantified after co-culture with 44v6.28ζ cells at 1:10 E:T ratio (see Methods for treatments*; n* = 3 to 6 donors). In (**D** to **F**), treatments were washed-out before functional assays and co-culture killing is expressed as elimination index (see Methods). (**G**) Schematics of T3M-4 pancreatic cancer (PAC) xenograft models are shown. In the minimal residual disease (MRD) setting, mice bearing T3M-4 tumors expressing a secreted luciferase (Luc^{+}) were injected i.p. with 2DG (500 mg/kg) or PBS on day 2 and 3 before treatment with 10 x 10^6 CAR T cells on day 3 (19.28ζ, *n* = 4 mice per group; 44v6.28ζ, *n* = 9 mice per group). In the high tumor burden (HTB) setting, mice bearing Luc^{+} T3M-4 tumors were injected i.p. with 2DG or PBS on day 6 and 7 before treatment with 5 x 10^6 CAR T cells on day 7 (19.28ζ, *n* = 5 mice per group; 44v6.28ζ, *n* = 4 mice per group). (**H**) Tumor growth was measured by bioluminescent analysis of blood samples. RLU, relative light unit. MRD, results from a two-way ANOVA are shown as 44v6.28ζ groups versus 19.28ζ groups. HTB, results from a two-way ANOVA are shown as 44v6.28ζ+2DG versus 19.28ζ+2DG. (**I**) Exhaustion marker SPICE analysis is shown for 44v6.28ζ cells retrieved from tumor masses 10 days after injection in mice from the HTB tumor setting from (H). IRs, inhibitory receptors; TILs, tumor-infiltrating lymphocytes. (**J**) Pull down of biotinylated surface proteins from T3M-4 extracellular membrane lysates show PD-L1 molecular weight shifts upon treatment with 2DG (4mM, 48 hours) or control PNGase F (representative of three experiments). (**K**) Frequency of PD-1 binding to PD-L1+T3M-4 cells is shown (*n* = 3 independent samples). T3M-4 cells were fixed and assayed for the capacity of binding to recombinant human PD-1 Fc protein. In (**D**, **E**, and **K**), Control and 2DG denote cells either untreated or exposed to 4mM 2DG for 48 hours, respectively. *P* values (**P* < 0.05; ***P*

951 < 0.01; ***P < 0.001; ****P < 0.0001) were determined by one-way ANOVA (**A, B, F**), two-way

952 ANOVA (**D**, **E**, **H**) or two-tailed *t*-test (**I** and **K**). Data are presented as mean ± s.e.m.

953

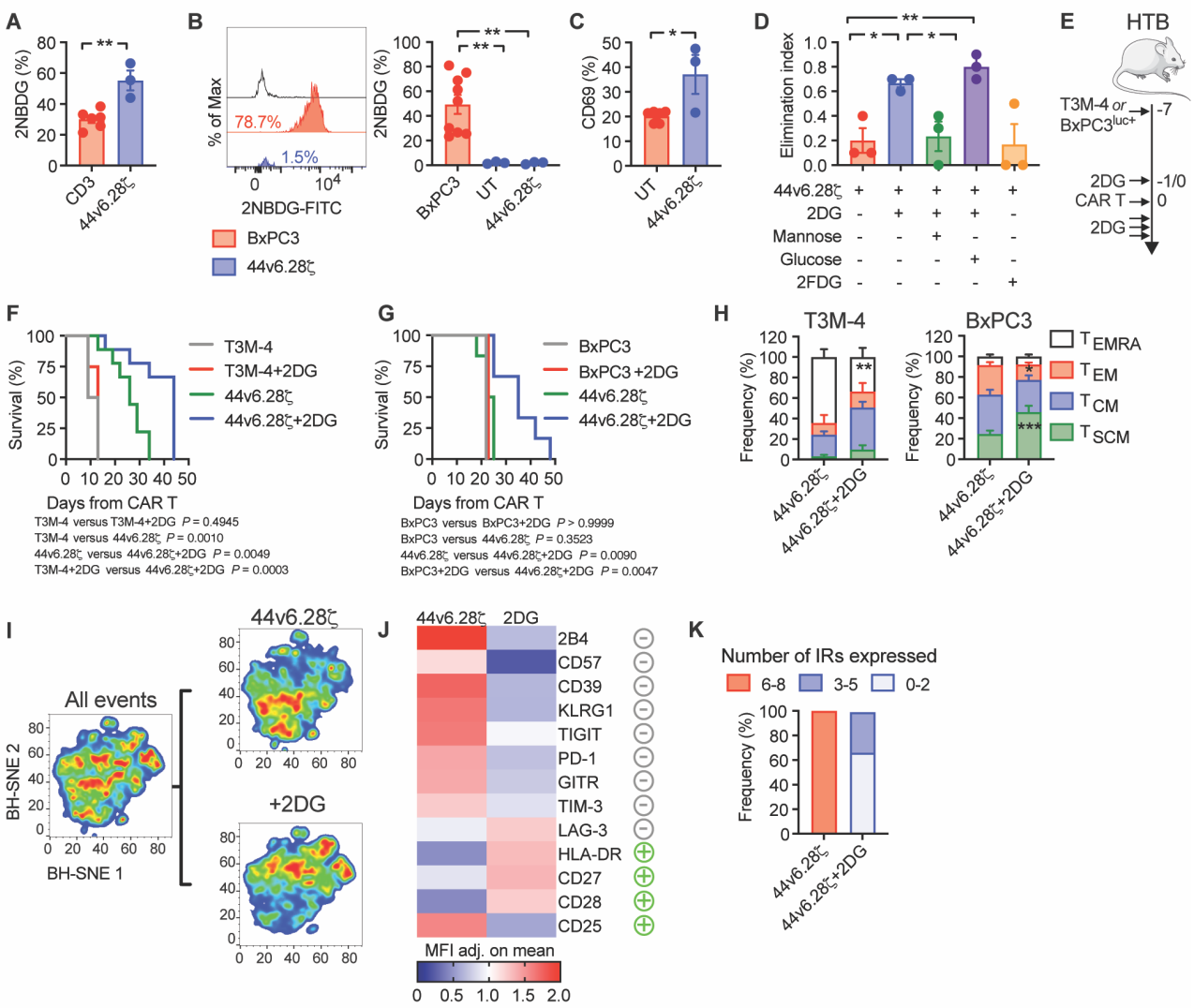

954

955 **Fig. 4. Co-treatment with 2DG enhances 44v6.28ζ cells potency and mitigates exhaustion in**
956 **xenograft models of pancreatic cancer.** (**A**) Frequency of 2NBDG uptake (100μM, 2 hours) is
957 shown for T cells from at least 3 donors. CD3 and 44v6.28ζ denote resting T cells and CAR T cells
958 stimulated with polyclonal αCD3/CD28 microbeads, respectively. (**B**) The frequency of 2NBDG
959 uptake in BxPC3 and T cells from co-culture is shown. Left, flow cytometric representative plot.
960 Negative control is shown in white. Right, 2NBDG uptake in three donors. (**C**) Frequency of CD69
961 expression is shown for 44v6.28ζ cells cocultured with BxPC3 (n = 3 donors). In (**B**) and (**C**), UT,
962 untransduced T cells. (**D**) Killing of T3M-4 cells was measured after co-culture with 44v6.28ζ cells
963 at a 1:10 E:T ratio (*n* = 3 donors). Treatments were not washed-out during co-culture and killing is
964 expressed as elimination index. (**E**) Schematics of the co-treatment regimen in luciferase (Luc^+) T3M-

4 and BxPc3 pancreatic cancer (PAC) xenograft models are shown. Briefly, mice bearing high tumor burdens (HTB) were treated with 44v6.28ζ ($6.5x10^6$ for the T3M-4 model, $3x10^6$ for the BxPC3 model) and injected i.p. with 2DG (500 mg/kg) or PBS daily. (**F**) A Kaplan–Meier survival plot is shown for mice with T3M-4 HTB (19.28ζ, $n = 4$ mice per group; 44v6.28ζ, $n = 9$ mice per group). (**G**) A Kaplan–Meier survival plot is shown for mice with BxPC3 HTB (19.28ζ, $n = 3$ mice per group; 44v6.28ζ, $n = 6$ mice per group). (**H**) The memory phenotype of circulating 44v6.28ζ cells was evaluated two weeks after infusion into mice from (**F**, left) and (**G**, right). (**I** to **K**) BH-SNE algorithm-mediated analysis of inhibitory and activation markers is shown for purified tumor-infiltrating 44v6.28ζ cells retrieved 14 days after infusion into HTB T3M-4 PAC xenografts co-treated with either PBS or 2DG ($n = 4$ mice per group). (**I)** BH-SNE plots identifying the localization of clusters defined by cytofluorimetric markers co-expression are shown. (**J)** Expression heat map are shown for clusters ascribed to specific experimental groups after K-means statistical analysis. Mean fluorescence intensity (MFI) values were normalized on the mean value. Negative grey circles, inhibitory markers. Positive green circles, activating markers. (**K**) The frequency of inhibitory receptor (IR) marker co-expression is shown for clusters enriched in either PBS or 2DG treatment. *P* values (*$P < 0.05$; **$P < 0.01$; ***$P < 0.001$) were determined by two-tailed *t*-test (**A**, **C**), one-way ANOVA (**B**, **D**), log-rank Mantel-Cox test (**F**, **G**) or two-way ANOVA (**H**). Data are presented as mean ± s.e.m.

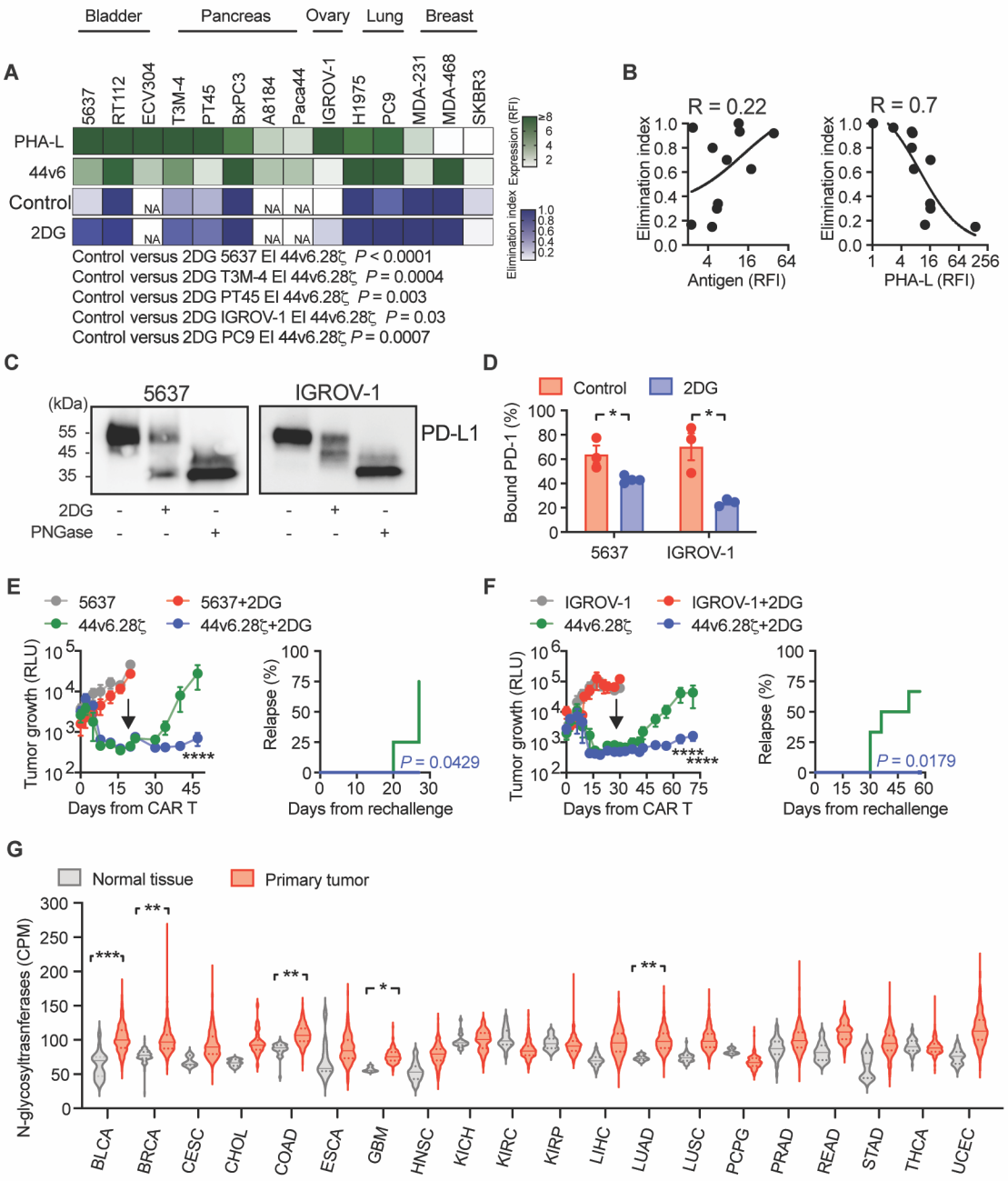

Fig. 5. Glycosylation blockade with 2DG is widely applicable to boost 44v6.28ζ cells against multiple solid tumors. (**A**) The heat map depicts expression (RFI, relative fluorescence intensity) of branched N-glycans (PHA-L) and CD44v6 on a panel of tumor cells lines (green lines) and target cell killing (elimination index) after co-culture with CAR T cells alone (Control) or in combination with 2DG at 1:5 effector:target E:T ratio (blue lines). NA, not applicable. (**B**) Pearson correlation analysis is shown for CD44v6 (left) or N-glycans (PHA-L, right) expression and killing by 44v6.28ζ cells. Analysis was performed on antigen-positive tumors (RFI ≥ 2). (**C**) Pull down of biotinylated surface

proteins from 5637 and IGROV-1 extracellular membrane lysates shows PD-L1 molecular weight shifts upon treatment with 2DG (4mM, 48h) or control PNGase F (representative of three experiments). (**D**) Frequency of PD-1 binding to PD-L1$^+$ tumor cells was quantified from 3 independent samples. Tumor cells were fixed and assayed for the capacity of binding to recombinant human PD-1 Fc protein. In (**A** and **D**), Control and 2DG denote cells either untreated or exposed to 4mM 2DG for 48 hours, respectively. (**E**) Tumor growth and relapse incidence was measured after tumor rechallenge of mice injected with luciferase (Luc$^+$) 5637 bladder tumor cells and infused with 4x10^6 CAR T cells on day 14 (only tumor, $n = 3$ mice per group; 44v6.28ζ, $n = 4$ to 5 mice per group). Tumor rechallenge (black arrow) was performed on day 20. (**F**) Tumor growth and relapse incidence was measured after tumor rechallenge of mice injected with Luc$^+$ IGROV-1 ovarian tumor cells and infused with 4.5x10^6 CAR T cells on day 7 (only tumor, $n = 3$ to 4 mice per group; 44v6.28ζ, $n = 6$ mice per group). Tumor rechallenge (black arrow) was performed on day 19. In (**E** and **F**), secreted luciferase was measured by bioluminescent analysis of blood samples. RLU, relative light unit. Mice received daily i.p. injections of either 2DG (500 mg/kg) or PBS. (**G**) Expression (counts per million) of N-glycans glycosyltransferases is shown in tumors and adjacent normal tissues from patients with different cancer types plotted using TCGA data. *P* values (*$P < 0.05$; **$P < 0.01$; ***$P < 0.001$; ****$P < 0.0001$) were determined by two-way ANOVA (**A**, **E**, **F**), non-linear regression curve fit (**B**), two-tailed *t*-test (**D**) or Fisher test (**G**). Data are presented as mean ± s.e.m.

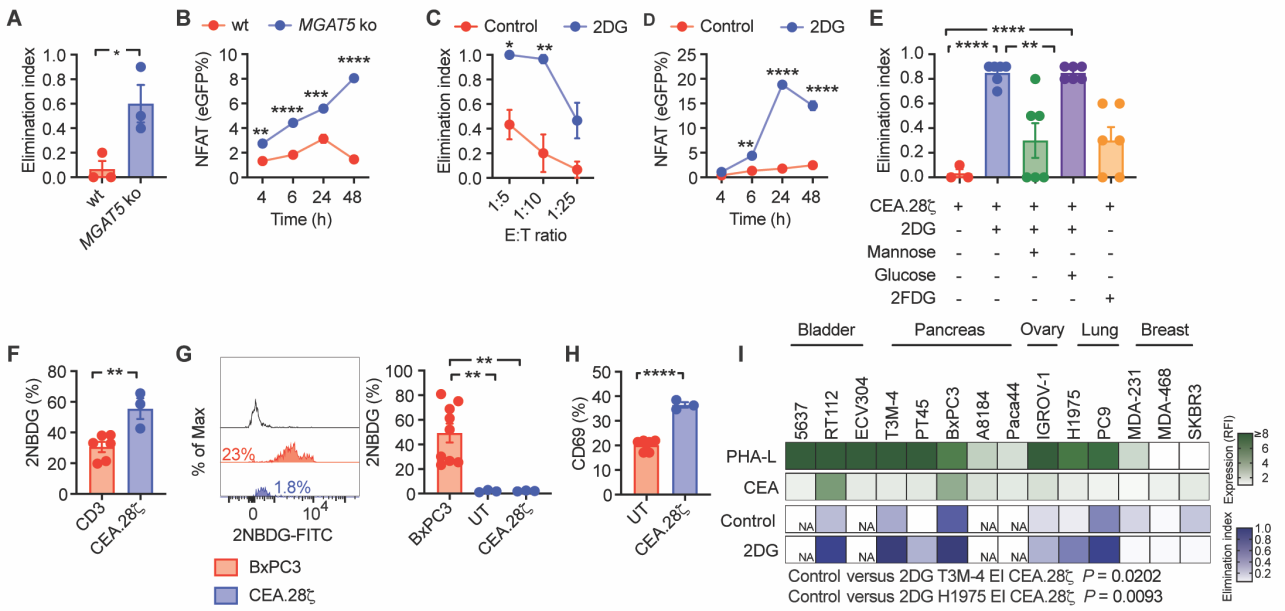

Fig. 6. Inhibition of N-glycan expression with 2DG boosts CEA.28ζ cell killing against different solid tumors. (**A**) Killing of T3M-4 cells was measured after co-culture with CEA.28ζ cells at the 1:10 effector:target (E:T) ratio (n = 3 donors). (**B**) Frequency of NFAT activation is shown in Jurkat TPR CEA.28ζ$^+$ cells during time-course stimulation with wt or *MGAT5* ko target cells (n = 3 independent samples). In (**A** and **B**), wt and *MGAT5* ko denote wild-type and *MGAT5* knocked-out T3M-4 cells, respectively. (**C**) Killing of T3M-4 cells was measured after co-culture with CEA.28ζ cells at different E:T ratios (n = 3 donors). **(D)** Frequency of NFAT activation is shown in Jurkat TPR CEA.28ζ$^+$ cells during time-course stimulation with untreated or 2DG-treated target cells (n = 3 independent samples). In (**C** and **D**), Control and 2DG denote T3M-4 cells either untreated or exposed to 4mM 2DG for 48 hours, respectively. (**E**) Killing of T3M-4 cells was measured after co-culture with CEA.28ζ cells at 1:10 E:T ratio after exposure to the indicated treatments (n = 3 to 6 donors). (**F**) Frequency of 2NBDG uptake (100μM, 2h) was measured in T cells from at least 3 donors. CD3 and CEA.28ζ denote resting T cells and CAR T cells stimulated with polyclonal αCD3/CD28 microbeads, respectively. (**G**) Frequency of 2NBDG uptake in BxPC3 and T cells was measured after co-culture. Left, flow cytometric representative plot. Negative control is shown in white. Right, 2NBDG uptake in three donors. (**H**) Frequency of CD69 expression was measured in CEA.28ζ cells

co-cultured with BxPC3 cells (n = 3 donors). In (**G** and **H**), UT, untransduced T cells. (**I**) The heat map depicts expression (RFI, relative fluorescence intensity) of branched N-glycans (PHA-L) and CEA on a panel of tumor cells lines (green lines) and target cell killing after co-culture with CAR T cells alone (Control) or in combination with 2DG at 1:5 E:T ratio (blue lines). NA, not applicable. In (**A**, **C**, **E,** and **I**), killing is expressed as elimination index. In (**C**, **D**, and **I**), Control and 2DG denote cells either untreated or exposed to 4mM 2DG for 48 hours, respectively. In (**C**, **D**, **E**, and **I**), treatments were washed-out before assays. *P* values (*$P < 0.05$; **$P < 0.01$; ***$P < 0.001$; ****$P < 0.0001$) were determined by two-tailed *t*-test (**A, F**, **H**), two-way ANOVA (**B**, **C**, **D**, **I**) or one-way ANOVA (**E**, **G**). Data are presented as mean ± s.e.m.